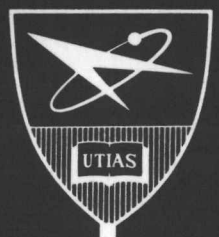

INSTITUTE
FOR
AEROSPACE STUDIES

UNIVERSITY OF TORONTO

DUCT EFFECTS ON THE DYNAMIC FAN CHARACTERISTICS OF AIR CUSHION SYSTEMS

by

M. J. Hinchey and P. A. Sullivan

June, 1977

UTIAS Technical Note No. 211
CN ISSN 0082-5263

DUCT EFFECTS ON THE DYNAMIC FAN CHARACTERISTICS OF AIR CUSHION SYSTEMS

by

M. J. Hinchey and P. A. Sullivan

Submitted December, 1976

June, 1977

UTIAS Technical Note No. 211
CN ISSN 0082-5263

Acknowledgements

This work was supported financially by the National Research Council of Canada and by Hover-Jak Limited through its IRAP program.

Abstract

During dynamic operation of an air cushion system, the fan operating point as seen at the cushion does not move along a static characteristic. Instead, it moves on a loop. Such loops have been observed experimentally by Durkin and Langhi (Ref. 1). This note shows that loop type behaviour can be predicted theoretically. The theory models the fan-duct-plenum system as a one dimensional acoustic vibration system. It uses the well known Method of Characteristics and a finite difference technique known as the method of specified time intervals to solve for the pressure and flow variations which occur along the duct during unsteady operation. Several practical situations where the loop behaviour may be of importance are discussed.

Contents

Notation

a	Sound speed
a_{ij}	Coefficients in Jacobian matrix
A_{ij}	Coefficients in inverse Jacobian matrix
A	Amplitude of pressure variation
A	Area
A_O	Valve flow area
A_{OI}	Amplitude of flow area variation of valve
A_{OO}	Mean flow area of valve
C_o, C_1, C_2	Coefficients in static fan characteristic
C_d	Discharge coefficient
C_P	Head coefficient
C_Q	Flow coefficient
C^+	C^+ characteristic line in x-t plane
C^-	C^- characteristic line in x-t plane
D	Diameter of duct
f	Friction factor
G	Gravitational acceleration
h	Hover-gap
J	Jacobian matrix
ℓ_P	Plenum perimeter
L	Length
N	Fan speed (rps)
P	Pressure
Q	Flow
R	Characteristic dimension of an orifice
R	Gas constant for air

Re	Reynolds number
S	Distance along streamline
S_b	Plenum cross-section at ground level
T	Temperature
t	Time
T_{NON}	A nondimensionalized time
V	Velocity
Ψ_c	Cushion volume
Ψ_o	Dead volume of cushion
x	Distance along duct from fan
ρ	Density
λ	Factor used in method of characteristics
τ_o	Friction stress at duct wall
ΔP	Pressure difference across an orifice
Δx	Space discretization
Δt	Time discretization
θ	$\Delta t/\Delta x$
ΔP_{fan}	Amplitude of pressure pulse at fan
γ	Polytropic exponent
ω	Frequency cps

Subscripts

b	Blade passing
co	Connecting orifice
d	Duct
e	Equilibrium
fan	Fan

f	Operating point
fe	Fan equilibrium
n	Natural
c	Plenum

1. INTRODUCTION

In Ref. 1, Durkin and Langhi presented experimental results which showed that during dynamic operation of a centrifugal fan the operating point (P_f, Q_f) does not move along a static characteristic. The test facility of Ref. 1 is shown schematically in Fig. 1. It consisted essentially of a centrifugal fan which discharged air into a plenum. Flow from the plenum was regulated by a rotating valve. The fan was of the HEBA type and was designed to operate at 3200 rpm while pumping 10,000 cfm of air against 100 psf. The facility is being used to investigate the static and dynamic performance of various fan systems for the proposed U.S. Navy 100-ton Surface Effect Ship (SES). The rotating valve simulates movement of the SES over a wavy sea. To establish the fan operating point, static pressure measurements were made at the volute exhaust, while flow measurements were made in the fan inlet. Flow measurements made in the volute and in the exhaust duct were found to be unreliable.

Typical results from Ref. 1 are shown in Figs. 2 to 4. Although not explicitly stated in Ref. 1, the data given indicate that the pressure and flow measurements were nondimensionalized according to standard fan laws, i.e., (see Notation)

$$\text{Head Coefficient} = C_P = \frac{P_f}{\rho N_{fan}^2 D_{fan}^2} \tag{1.1}$$

$$\text{Flow Coefficient} = C_Q = \frac{Q_f}{N_{fan} D_{fan}^3} \tag{1.2}$$

The results show some of the closed curves or loops (dynamic characteristics) along which the operating point moved after transients associated with start-up of the rotating valve had died away. The size and shape of the loops were found to be very much dependent on the valve frequency. For example, at the lower frequencies (e.g. Fig. 2), the deviation of the dynamic characteristics from the static characteristic was small, whereas, for the intermediate frequencies (e.g. Fig. 3), the deviation was large. Also, as the valve frequency was increased, the negative pitch of the loops became steeper (Fig. 4).

Note in Figs. 2 to 4 that there is an absence of scaling with respect to fan speed. This indicates that in a dynamic situation the standard fan laws by themselves are not adequate. In Ref. 1, the effect was attributed to the distinct DC pressure levels associated with each fan speed and the flow-limit crossover between the fan static curves and the rotating valve admittance curve. For example, at the higher fan speeds, it was felt that the fan probably controlled the flow to the plenum, whereas, at the lower speeds, the rotating valve admittance characteristic probably established the flow.

It was concluded that performance curves used to characterize steady operation of the fan do not describe the dynamic behaviour of the fan system - i.e., rotor, discharge volute, and plenum. Preliminary data analysis indicated that fluid inertia in the fan volute, compliance of air in the plenum, and compliance of the plenum walls were probably responsible for most of the loop behaviour. Other factors which may have had some effect are: fan rotor inertia,

fan blade stall, inertia of the air in the inlet, inertia of the air in the exhaust duct, leakage of air from the volute back into the inlet due to inadequate sealing between the inlet bellmouth and the fan impeller, and leakage of air from the plenum.

This note shows that loops, similar to those shown in Figs. 2 to 4, can be predicted theoretically. The theory, which was developed for the system shown in Fig. 5, takes into account the inertia and compressibility of the air in the duct and the compressibility of the air in the plenum. The analysis is one dinensional in that it assumes that, at any position x along the ducting, conditions are uniform across the cross-section normal to the duct axis. The theoretical development follows very closely that presented for hydraulic transients by Streeter and Wylie (Ref. 2). It uses the well known method of characteristics and a finite difference technique known as the method of specified time intervals. The characteristics method was used instead of other methods such as the equally well-known and somewhat simpler impedance methods (Ref. 2, p. 101) for two reasons. Firstly, one aim was to investigate the initial start-up transients associated with the first few oscillations of the valve. Also, for the large valve area variations contemplated, it was felt necessary to use nonlinear boundary conditions. The characteristics method can include both of the above, whereas the impedance method cannot. The details of the analysis are given in Appendix A. The computer program is given in Appendix B. For all of the results obtained, the fan operating point was defined as the pressure and flow immediately upstream of the connecting orifice (see Fig. 5).

2. OUTLINE OF THE THEORY AND ITS ASSUMPTIONS

2.1 Outline of Theory

The two partial differential equations governing the one dimensional flow of air in a duct are (see Notation; Fig. 5):

Conservation of Momentum

$$\frac{\partial P}{\partial x} + \rho_e \frac{fV|V|}{2D} + \rho_e V \frac{\partial V}{\partial x} + \rho_e \frac{\partial V}{\partial t} = 0 \qquad (2.1)$$

Conservation of Mass (Continuity)

$$\rho_e \frac{\partial V}{\partial x} + \frac{1}{a^2}\left(V \frac{\partial P}{\partial x} + \frac{\partial P}{\partial t} \right) = 0 \qquad (2.2)$$

For Eq. (2.2), the compression-expansion processes were assumed to behave polytropically. The equations are quasi-linear and hyperbolic. Because of their hyperbolic nature, they can be reduced to ordinary differential equations by the method of characteristics. The ordinary differential equations are:

$$\left.\begin{aligned} \rho_e \frac{dV}{dt} + \frac{1}{a}\frac{dP}{dt} + \rho_e \frac{fV|V|}{2D} &= 0 \qquad (2.3) \\ \text{on } \frac{dx}{dt} &= V + a \qquad (2.4) \end{aligned}\right\} C^+$$

$$\left.\begin{aligned} \rho_e \frac{dV}{dt} - \frac{1}{a}\frac{dP}{dt} + \rho_e \frac{fV|V|}{2D} &= 0 \qquad (2.5) \\ \text{on } \frac{dx}{dt} &= V - a \qquad (2.6) \end{aligned}\right\} C^-$$

Equations (2.4) and (2.6) describe characteristic lines in the x-t plane along which Eqs. (2.3) and (2.5) are valid. The C^+ pair of equations are associated with the C^+ characteristic, and the C^- pair are associated with the C^- characteristic. A sketch of the characteristic lines is shown in Fig. 6. They are almost straight lines in the present application because $V + a \cong a$. If conditions are known at positions R and S in the x-t plane, then conditions at position P can be obtained by integrating numerically equations (2.3) and (2.5) along their respective characteristic line.

The ordinary differential equation system can be solved numerically by any one of a number of finite difference techniques. The technique used here is known as the method of specified time intervals (Ref. 2, p. 32). For this, the discretizations of space and time are specified. The procedure, which is very much like an Euler integration, leads to an orderly numerical solution on a digital computer. The finite difference forms of the equations are (see Fig. 6):

$$V_P - V_R + \frac{1}{\rho_{R_e}} \frac{(P_P - P_R)}{a} + \frac{f}{2D} V_R |V_R| (t_P - t_R) = 0 \qquad (2.3)'$$

$$x_P - x_R = (V_R + a)(t_P - t_R) \qquad (2.4)'$$

$$V_P - V_S - \frac{1}{\rho_{S_e}} \frac{(P_P - P_S)}{a} + \frac{f}{2D} V_S |V_S| (t_P - t_S) = 0 \qquad (2.5)'$$

$$x_P - x_S = (V_S - a)(t_P - t_S) \qquad (2.6)'$$

At time t, conditions are known at positions A, C, and B. Conditions at R and S are obtained using Eqs. (2.4)' and (2.6)' and a linear interpolation. With known conditions at R and S, conditions at position P are then obtained from Eqs. (2.3)' and (2.5)'.

For all but a few of the theoretical results obtained, a static fan characteristic of the form (implies no loop at fan)

$$P_{fan} = C_o + C_1 V_{fan} + C_2 V_{fan}^2 \qquad (2.7)$$

was used as the upstream boundary condition on the duct flow. Quasi-steady, inviscid incompressible, orifice flow equations of the form

$$Q = C_d A \sqrt{\frac{2\Delta P}{\rho_e}} \tag{2.8}$$

were used as boundary conditions at the connecting orifice and at the variable orifice.

Figures 7 and 8, from Ref. 2, show some applications of the characteristics theory to hydraulic transients. The agreement between theory and experiment can be seen to be very good. In Ref. 3, it was shown that the theory could also be used to calculate the transients which occur in the piping connecting a supercharger and the manifold of an internal combustion engine.

2.2 Discussion of Assumptions

In Section 2.1, a number of assumptions were employed. For example, for the conservation of momentum equation, it was assumed that the friction force acting on a fluid element due to its motion relative to the duct was of the Darcy Weisbach type. For this, the flow must be turbulent. Here, a typical Reynolds number for the duct flow is Re = 100,000. So, the friction force assumption should be adequate. The results presented in Ref. 2 indicate that it is a reasonable assumption. For the conservation of mass equation, we assumed that the thermodynamic compression-expansion processes were polytropic. This assumption introduced the sound speed into the analysis. Its limits are the isentropic and isothermal approximations. By definition, an isentropic process is one that is adiabatic and frictionless, whereas an isothermal process is a constant temperature process. Now, as mentioned above, the duct flow in the present case is turbulent. Thus, the flow will be dissipative and not frictionless. However, it can be shown that, here, the work done on a typical fluid element by the friction force is small order of the work done by the pressure force. So, at least in this respect, the flow should behave as if it were frictionless. Also, arguments presented in Ref. 4 indicate that heat conduction along the duct will not be significant for the frequency range considered in this report. Thus, if we assume no heat flow through the duct walls, the thermodynamic processes should be approximately adiabatic. From the above, we conclude that the compression-expansion processes for the duct flow are approximately isentropic. Similar arguments indicate that the compression-expansion processes occurring within the plenum are also approximately isentropic.

Another assumption, mentioned previously, is that the flow is one dimensional. For the duct flow, there are two reasons why this should be a good assumption. First, the flow is turbulent. Thus, conditions should be uniform across cross-sections normal to the duct axis. Second, the duct length to diameter ratio is sufficiently large. However, for the plenum, where, here, the length to diameter ratio is only 0.5, the assumption is not valid. The flow in this case is known to be at least two dimensional (Ref. 5). Vortices, formed by entrainment of air by the inlet orifice feed jet, are usually present. Thus, it is to be expected that nothing would be gained by using the method of characteristics approach for the plenum flow. In fact, because, as will be shown later, the characteristics approach indicates that there is very little variation of pressure along the plenum, one would expect that the standard

lumped volume approach would be just as adequate. Both approaches were used and were found to give nearly identical results. This indicates that, in the limit as the plenum or duct length becomes very short relative to its diameter, the method of characteristics approach goes over naturally to the standard lumped volume approach. In Appendix A, the characteristics approach is used for the duct flow and the lumped volume approach is used for the plenum.

Finally, it must be remembered that the inviscid incompressible orifice flow equation (Eq. 2.8),used as the duct downstream boundary condition, is a steady-state equation. It is derived from Euler's equation, i.e.,

$$\rho \underbrace{\frac{\partial V}{\partial t}}_{\substack{\text{local} \\ \text{term}}} + \rho V \underbrace{\frac{\partial V}{\partial S}}_{\substack{\text{convective} \\ \text{term}}} + \frac{\partial P}{\partial S} = 0 \qquad (2.9)$$

by assuming the flow to be steady and ρ to be constant, i.e.,

$$\rho_e V \frac{dV}{dS} + \frac{dP}{dS} = 0 \qquad (2.10)$$

Integrating Eq. (2.10) with respect to S gives Bernoulli's equation, i.e.,

$$\frac{1}{2} \rho_e V^2 + P = \text{constant} \qquad (2.11)$$

from which

$$Q = C_d A V_c = C_d A \sqrt{\frac{2\Delta P}{\rho_e}} \qquad (2.8)$$

follows directly. For this equation to be applicable in a dynamic situation, two conditions must be met. First, the time required for a pressure change on either side of the orifice to propagate the extent of the orifice must be small compared to the time for one cycle of oscillation of the valve. Second, the local acceleration term in Euler's equation must be small compared to the convective term. With regard to the first condition, it is known that the time required for a pressure change to propagate the extent of the orifice is of the order of the time required for a sound wave to travel the extent of the orifice. For the present work, this time is of the order of 5×10^{-4} seconds or less. For most of the results obtained, the valve frequency was $\omega = 5$ cps. Thus, the time for one valve oscillation was on the average 0.2 seconds. Thus, as the wave propagation time was on the average only 0.25% of the valve oscillation time, we can assume that the first condition has been satisfied. With regard to the second condition, it is known from potential flow theory that, at distances greater than about one characteristic length (hover-gap or orifice radius) upstream of an orifice, the flow is very much like sink flow (Ref. 6). The streamlines are almost radial and form reasonably well-defined channels. Thus, for steady flow, we can use simple continuity arguments for flow in converging channels to relate approximately the velocities at various radial positions. We find

$$V \simeq f(S, R, V_c) \tag{2.12}$$

where S is the distance along an orifice streamline, R is the characteristic dimension of the orifice, and V_c is the velocity at some selected point. Here, we choose for this point the vena contracta of the orifice where

$$V_c = \sqrt{\frac{2\Delta P}{\rho_e}} \tag{2.13}$$

Now, if we assume that Eqs. (2.12) and (2.13) are valid in the dynamic situation, then we can estimate the magnitudes of the local and convective accelerations appearing in Eq. (2.9). This is done as follows. First, we let the driving pressure ΔP vary sinusoidally according to

$$\Delta P = \underset{\text{mean}}{\Delta P_e} + \underset{\text{perturbation}}{A \sin(2\pi \omega t)} \tag{2.14}$$

Substituting Eq. (2.14) into Eq. (2.13) and then Eq. (2.13) into Eq. (2.12) gives an expression for V as a function of time. Thus, by differentiation, we have $\partial V/\partial t$. Similarly, as we know V as a function of S, we can also calculate $V\,\partial V/\partial S$. Taking only the maximum value of each of these terms, we can form the ratio

$$R_{L/C} = \frac{\text{Maximum Local Acceleration}}{\text{Maximum Convective Acceleration}} \tag{2.15}$$

If this calculation shows that the local term is on the average much smaller than the convective term, then use of Eq. (2.8) will be justified. Calculations of this type show that, here, for the valve (slot orifice), $R_{L/C}$ was on the average only 0.005 (0.5%). Thus, for the valve, Eq. (2.8) was adequate. However, for the connecting orifice (circular orifice), the calculations show that $R_{L/C}$ was on the average as much as 0.15 (15%). The percentages were found to increase linearly with valve frequency. The values given above were for ω = 5cps. For ω = 20 cps, the percentages were 2% and 60%. This result indicates that use of Eq. (2.8) for the connecting orifice when ω was of the order of 20 cps was not justified. The errors present at ω = 5 cps are probably tolerable. $R_{L/C}$ was found to depend linearly on the characteristic dimension of the orifice, i.e.,

$$R_{L/C} \propto \frac{R\omega}{V_{ce}} \tag{2.16}$$

For the valve (slot orifice), the characteristic dimension is the slot width (here the hover-gap). For the connecting orifice (circular orifice), the characteristic dimension is the radius of the orifice. This explains why there is such a large difference between $R_{L/C}$ for the valve and $R_{L/C}$ for the connecting orifice.

3. RESULTS

3.1 System Geometry

The system of Ref. 1 differs appreciably from the model of Fig. 5. So, any application of the characteristics theory developed here to it would be very approximate. The results presented here are for a system which resembles closely the theoretical model. The system considered is the basic component of a Canadian ACV raft known as the HJ-15 and consists of one slightly tapered cell connected to a fan by a duct. Its dimensions are given in Table 1.

Table 1

Geometry of HJ-15 Cell

Average Diameter of Cell	$\cong$	1.83 metres (6.0 feet)
Height of Cell	$\cong$	0.915 metres (3.0 feet)
Inlet Feed Orifice Diameter	=	0.305 metres (1.0 foot)
Diameter of Duct	=	0.457 metres (1.5 feet)
Typical Hover-gap	=	0.636 cm (1/4 inch) (Reference)
Duct Friction Factor	=	0.07 (Reference)
Duct Length	=	7.62 metres (25 feet) (Reference)
Amplitude of Hover-gap Variation	=	0.318 cm (1/8 inch) (Reference)
Polytropic Exponent	=	1.4 (Reference)
Fan Speed	=	28.3 rps (1700 rpm)
Fan Impeller Diameter	=	1.25 metres (4.08 feet)

3.2 General Features of the Results

The results were obtained by varying the valve area according to the relation

$$A_o = A_{oI} \sin(2\pi \omega t) + A_{oo} \qquad (3.1)$$

where, at time $t = 0$, conditions throughout the system were steady. Most of the results show the final closed loops along which the operating point moves after transients associated with start-up of the valve have died away. As mentioned

previously, here, the operating point is defined as the pressure and flow immediately upstream of the connecting orifice. Note that this definition is slightly different from that of Ref. 1. Also, the pressure-flow results have been nondimensionalized according to standard fan laws. For all results, the mean flow area of the valve (i.e., A_{oo}) was equal to the exit area from the cell when it is operating at a hover-gap of 0.64 cm (1/4"). Also, the starting values of C_P and C_Q were the same (or nearly the same) for all results presented. The numerical accuracy of the results was checked by refining the x-t grid and was found to be adequate (less than 0.1% error).

Some typical theoretical results are shown in Fig. 9. For these, the duct length is typical for HJ-15 cells which are far from the fan. Also, $A_{oI} = A_{oo}/2$. This corresponds to a heave motion of amplitude 0.32 cm (1/8"). At the upstream end of the duct a constant pressure source was imposed. The arrow pointing along any given loop indicates the sense in which the operating point is moving. For example, for the $\omega = 1$ cps result, the operating point is moving in a counter-clockwise sense. The arrow approximately normal to the loop and pointing at a specific point on the loop indicates the position of the operating point at the beginning of the fifth cycle of oscillation of the valve (at this point $A_o = A_{oo}$). This gives some idea of the phase relationship between the operating point motion and the valve motion. The results can be seen to resemble in many respects those presented in Ref. 1. For example, at the lower frequency (i.e., $\omega = 1$ cps), the deviation of the dynamic characteristic from the static characteristic is not very large. As the frequency of valve motion increases, the deviation at first increases and then decreases. Also, the negative pitch of the loops becomes steeper as ω is increased. The arrows normal to the loops show that the operating point motion tends to lag the valve motion as the valve frequency is increased. This lagging is probably due mostly to the inertia of the air in the duct. Because of the inertia, time is required to accelerate and decelerate the flow. The result is a tendency for the flow to lag the pressure.

It is also apparent that the pressure fluctuations peak at a certain valve frequency (Fig. 10). This effect is discussed in Ref. 2 as follows. It is known that the time taken for a pressure wave to travel the length of a pipe of length L is

$$t = \frac{L}{a} \tag{3.2}$$

Associated with this time is a pipe natural frequency given by

$$\omega_n = \frac{1}{4t} \tag{3.3}$$

For a 7.62 metre pipe, $\omega_n \cong 11$ cps ($\gamma = 1.4$). When the pipe flow is forced at frequency ω_n by a rotating valve at the downstream end, a velocity node and pressure peak occur immediately upstream of the valve. In other words, for this frequency, the flow at the valve is essentially fixed while the pressure fluctuations attain their maximum value; the pressure-flow operating point moves up and down on a vertical line. Now, for a series system in which the downstream pipe has a much larger cross-section than the upstream pipe, the situation is much more complex. For this, it is found that, whereas a velocity node still occurs at the pipe junction when the valve frequency is around ω_n,

the pressure at the junction does not peak at ω_n. Instead, the pressure peaks at a much lower frequency. This is basically what is happening in Figs. 9 and 10.

Figures 11 and 12 show some of the results of Fig. 9 in more detail. Figure 11a, for example, shows some of the initial transients associated with start-up of the valve. The general trend is that, as the valve frequency is increased, the transients persist for more cycles of oscillation. Figure 11b gives plots of C_P and C_Q versus a nondimensionalized time T_{NON} where

$$T_{NON} = t\,\omega \tag{3.4}$$

T_{NON} is basically just the number of cycles of valve oscillation completed. Besides showing transients associated with valve start-up, the results show clearly how the phase relationships of the pressure and flow with respect to valve motion vary with valve frequency. Figure 12a shows how the pressure varies with distance along the duct and the plenum when the operating point pressure is at its maximum value. For these results, a computer program in which both the duct and the plenum were modelled by the characteristics approach was used. For oscillations of the valve at frequencies higher than ω_n, one can see that the maximum pressure fluctuations do not occur immediately upstream of the connecting orifice. Also, these results show that the variation of pressure with distance along the plenum is very small. This, as mentioned previously, indicates that, for the plenum, a lumped volume approach is adequate. Figures 12b and 12c compare loop shapes at different positions along the duct.

3.3 Effects of Varying Selected System Parameters

Figure 13 gives typical loops obtained with a duct of length 3.04 metres (10 feet). This length is typical for HJ-15 cells which are situated close to the fan. All other system dimensions were the same as those for Fig. 9. For the results, a typical static fan characteristic was imposed at the upstream end of the duct (fan). The results can be seen to display characteristics similar to those of Fig. 9. The most noticeable difference is that here the deviations of the dynamic characteristics from the static characteristic are much smaller. This is to be expected because, in the limit as the duct length goes to zero, the differences between static and dynamic characteristics must also go to zero. This is because we have imposed a static characteristic at the fan.

Figure 14a shows a polytropic exponent effect. For this, the reference is the $\omega = 5$ cps result of Fig. 9 for which the polytropic exponent was $\gamma = 1.4$ (isentropic). The polytropic exponent enters into the analysis through the definition of the sound speed, i.e.,

$$a = \sqrt{\gamma RT} \tag{3.5}$$

Because it affects the sound speed, it also affects the duct natural frequency ω_n through

$$\omega_n = \frac{a}{4L_d} \tag{3.6}$$

and the amplitude of the pressure fluctuations through (see Appendix A)

$$\Delta P \cong \frac{\rho_{ce}\, a}{2} (V_R - V_S) \tag{3.7}$$

where ΔP is the change in pressure at a particular point in the duct over one time step (friction ignored).

Equation (3.6) indicates that, for the isothermal case ($\gamma = 1.0$), the natural frequency should be approximately 84% of ω_n for $\gamma = 1.4$, whereas Eq. (3.7) indicates that the amplitude of the pressure fluctuations should be smaller for the isothermal case. The results presented in Fig. 14 show that the natural frequency for the isothermal case is approximately 80% of ω_n for $\gamma = 1.4$, while the amplitude of the pressure fluctuations for the isothermal case is approximately 87% of the amplitude obtained for $\gamma = 1.4$. Thus, the arguments just used to explain the polytropic exponent effect are in agreement with the results obtained.

Figure 15 shows that the friction factor does not have a significant effect. This indicates that the motion of a fluid element is dominated by the pressure gradient force and not by the friction force. So, during steady oscillations, we have basically just a balance of inertia and pressure forces. If we consider the air in the duct as a whole, the results show that the maximum pressure force acting on this air is of the order of 155.5 newtons (35 lbs), whereas the friction force is of the order of 3.55 newtons (0.8 lbs). Thus, the results of Fig. 15 are not surprising.

When the hover-gap of a plenum type air cushion varies, the cushion volume also varies. This can be seen from

$$\forall_c = \underbrace{\forall_o}_{\substack{\text{dead} \\ \text{volume}}} + \underbrace{S_b}_{\substack{\text{plenum} \\ \text{cross-section} \\ \text{at ground} \\ \text{level}}} \underbrace{h}_{\substack{\text{hover-gap}}} \tag{3.8}$$

For all but a few of the results obtained, this change in volume was not accounted for. Figure 16 shows that its effect is significant. Here, the cushion volume changed by only 0.35% of its equilibrium value. This indicates that, for air cushions which experience large changes in cushion volume, the effect could be very large. This situation might occur for example in overwater operation when there is wave pumping.

Figure 17 shows the effect of doubling the amplitude of area variation of the variable orifice. As mentioned previously, $A_{oI} = A_{oo}/2$ corresponds to a heave motion of amplitude 0.32 cm (1/8"). Thus, here we are examining the effect of increasing this amplitude to 0.64 cm (1/4"). In Fig. 17, there are two important effects to note. First, the amplitude of the pressure fluctuations for the $A_{oI} = A_{oo}$ case is approximately double that obtained for $A_{oI} = A_{oo}/2$. Second, for the $A_{oI} = A_{oo}$ case, there is, at times, reverse flow at the connecting orifice. For this case, there was also reverse flow at the fan. It is obvious that this could have important consequences in practice. Figure 18 shows the loop obtained with $A_{oI} = A_{oo}/100$. This result is very important because it shows that, even when the amplitude of the area variations is very small, loops, similar in form to those obtained for large area variations, still occur. In Section 3.4, we show

that this may have important consequences for linear heave stability studies, where we deal with the amplification or decay of small disturbances to an air cushion system. Table 2 summarizes some of the results of Figs. 17 and 18. It shows that, contrary to what might have been expected, the output ΔC_P is almost linearly related to the input ΔA. The reason for this is not clear.

Table 2

Summary of Results of Figures 17 and 18

Input ΔA %	Output ΔC_P %	$\frac{\text{Output}}{\text{Input}}$
2	2.04	1.02
100	105	1.05
200	208	1.04

$$\Delta A = \frac{2A_{oI}}{A_{oo}} = \frac{\text{Peak to Peak Area Variation}}{\text{Mean Area}}$$

$$\Delta C_P = \frac{C_{P_{max}} - C_{P_{min}}}{C_{P_{mean}}} = \frac{\text{Peak to Peak } C_P \text{ Variation}}{\text{Mean Value of } C_P}$$

For the results presented so far, a static characteristic of the form

$$P_{fan} = C_o + C_1 V_{fan} + C_2 V_{fan}^2 \qquad (2.7)$$

was imposed at the fan. However, just immediately downstream of the fan blades, there may be small pressure and flow fluctuations associated with the fan blade motion. This blade passing frequency effect can be simulated by replacing Eq. (2.7) by

$$P_{fan} = \overline{P_{fan}} + \Delta P_{fan} \sin(2\pi \omega_b t) \qquad (3.9)$$

$\overline{P_{fan}}$ is the equilibrium or mean value of the fan pressure. ω_b is the blade passing frequency. The boundary condition imposes at the fan a small sinusoidal pressure disturbance. With P_{fan} known as a function of time, V_{fan} can be obtained directly from the C^- characteristic equation (see Appendix A, Section A3). Figure 19 shows a typical result obtained with the small pressure oscillation imposed at the fan. For this, we let $\omega_b = \omega = 5$ cps and $\Delta P_{fan} = 1$ psf. Note that, in this case, a pressure-flow loop occurs at the fan. It appears that the small loop at the fan does not have a significant effect on the loop shape at the connecting

orifice. This is important because it suggests that, for the present work, fan boundary conditions of the form given by Eq. (2.7) are adequate.

Figure 20 compares two loops for which the nondimensional static characteristics at the connecting orifice were the same but for which the dimensional values of pressure and flow were different. The comparison shows the failure of the fan scaling laws, and it agrees with the comparisons presented in Ref. 1. The failure to scale is probably due to the dynamic nature of the situation. For example, when one uses an impedance method (see Ref. 2), similar to that used to study steady voltage-current fluctuations on a transmission line, one finds that the impedance of the duct system is a 'complex' function of the forcing frequency, the physical properties of the duct, and the boundary conditions. The boundary conditions contain equilibrium values of pressure and flow velocity. Thus, the impedance of the duct depends in a complex way on the DC pressure levels. So, it is not surprising that fan scaling laws developed for the steady performance of fan systems break down here. Another reason for the failure to scale is that there are two characteristic periods for the system. One is associated with the fan speed while the other is associated with the duct length.

3.4 Situations where the Loop Behaviour may be of Importance

Figure 21 shows schematically the UTIAS heave table facility. This facility was used recently to study the static and dynamic performance of a TACV system known as the Hinged Lip Model (Ref. 7). As can be seen in Fig. 21, the model was connected to a fan by a long duct. To determine whether or not the long duct had a significant effect on the model's frequency response, several tests were performed with a large tank placed at the end of the duct, as shown. As mentioned in Ref. 2, the large volume of such a tank should reduce pressure fluctuations associated with the duct. Some typical comparisons of results obtained with and without the tank are given in Table 3. As expected, the most noticeable effect of the tank is a large reduction in the percentage pressure fluctuations about the equilibrium pressure. For the case where the bag feed area was only one tenth of the cushion feed area (highly damped case), the tank limited the rms value of the model heave motion at resonance to approximately 65% of the rms value obtained without the tank. For the case where the bag feed area was three times the cushion feed area (lightly damped case), the tank did not have much of an effect. Note the large pressure peaks which occur at approximately three times the natural frequency of the system when the tank is not installed. A possible explanation for these is the following. In Ref. 2, it is shown that, for a single pipe with an oscillating valve at the downstream end, the pressure immediately upstream of the valve will peak at the odd harmonics, i.e., $3\omega_n$, $5\omega_n$, etc. However, when a very large volume is placed between the pipe and the valve, these odd harmonics do not appear. The volume in this case acts as a filter. This seems to be what is occurring in the results of Table 2. The conclusion to be drawn from this is that frequency response results obtained from model tests should not be applied to actual systems when there are appreciable differences between the model ducting and the ducting present in the real system.

As a final example, consider the heave stability of an air cushion system. For linear, lumped-parameter, heave stability analyses, it is usual to assume that the pressure-flow operating point immediately upstream of the inlet feed orifice moves on a static characteristic. Typical examples of such characteristics are shown in Fig. 22a. We know from Fig. 18 that, even when the hover-gap variations are very small, the operating point does not move along

Table 3

Hinged Lip Results

System Geometry \ Result		Bode Plot $\frac{Y_{RMS}}{Z_{RMS}}$ db at Resonance	Pressure Fluctuation Expressed as % of Equilibrium Pressure -Resonance	Pressure Fluctuation at twice ω_n	Pressure Fluctuation at three times ω_n
$\frac{\text{Bag Feed}}{\text{Cushion Feed}} = \frac{3}{1}$	With Tank	14.5 db	7%	2%	2%
	Without Tank	14.5 db	29%	4%	17%
$\frac{\text{Bag Feed}}{\text{Cushion Feed}} = \frac{1}{10}$	With Tank	7.0 db	4.5%	2.5%	3%
	Without Tank	11.0 db	17.5%	6%	16%

such a characteristic. Instead, it moves on a loop. The shape of the loop along which the operating point moves depends very much on the natural frequency of the air cushion. This is because the system will tend to oscillate at this frequency. For example, if the natural frequency of the cushion ω_n is much lower than the duct natural frequency ω_d, then the operating point will move on a loop which does not deviate much from the static characteristic. Thus, in this case, if the static characteristic is a constant pressure source, then the loop will closely approximate such a source (Fig. 22b - $\omega_n \ll \omega_d$). On the other hand, if the natural frequency of the cushion is of the order of the duct natural frequency, then the loop for a constant pressure source will not closely approximate such a source. Instead, the loop will approximate a constant flow source (Fig. 22b - $\omega_n = O(\omega_d)$). Figure 23 shows typical lumped parameter heave stability boundaries for a HJ-15 cell. These were obtained using the linear heave stability analysis of the system presented in Appendix D of Ref. 5. The point to note in Fig. 23 is that, as the hover-gap goes to zero, a constant pressure source tends to give infinite stability, whereas a constant flow source tends to give no stability. Thus, one can see that, if the cushion natural frequency is such that small heave oscillations generate a loop which approximates a constant flow source, then stability results obtained assuming the operating point to move on a constant pressure static characteristic could be very much in error.

4. CONCLUSIONS

This note has shown that the dynamic fan characteristics of an air cushion system can differ appreciably from its static characteristic. The differences were found to be associated with the ducting connecting the fan and the air cushion. It is thus concluded that care must be exercised in applying theoretical or experimental results to actual systems when there are appreciable differences between the model ducting and the ducting present in the real system.

REFERENCES

1. Durkin, J. Langhi, W. — An Investigation of the Performance of a Centrifugal Lift Fan Operating Against Sinusoidally Varying Back Pressure. Canadian Air Cushion Technology Symposium, September, 1974.

2. Streeter, V. Wylie, B. — Hydraulic Transients. McGraw-Hill, 1967.

3. Benson, R. Whitfield, A. — An Experimental Investigation of the Non-Steady Flow Characteristics of a Centrifugal Compressor. University of Manchester, Institute of Science and Technology, September, 1965.

4. Morse, P. M. Ingard, K. U. — Theoretical Acoustics. McGraw-Hill, 1968.

5. Hinchey, M. — Heave Instabilities of Air Cushion Suspension Systems - Part 1. Hover-Jak, TN-75-5, 1975.

6. Birkhoff, G. Zarantonello, E. — Jets, Wakes, and Cavities. Academic Press, 1957.

7. Parravano, J. — Investigation of the Dynamic Response Characteristics of a Hinged Lip Air Cushion Suspension. M.A.Sc. Thesis, University of Toronto, December, 1976.

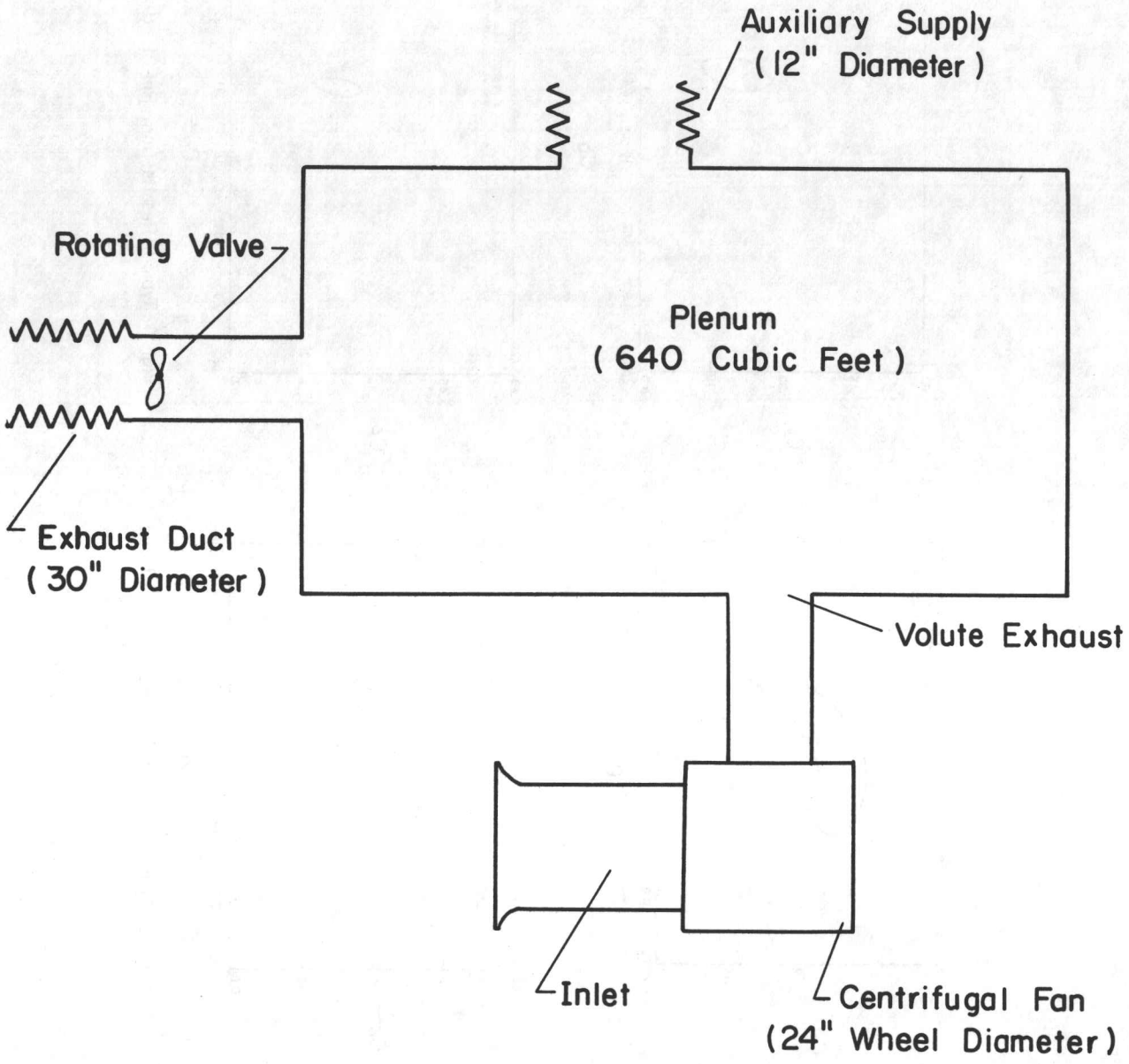

Fig. 1 Sketch of Experimental Facility of Ref. 1

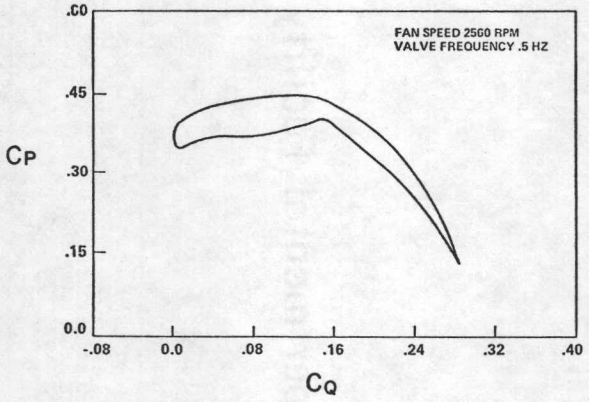

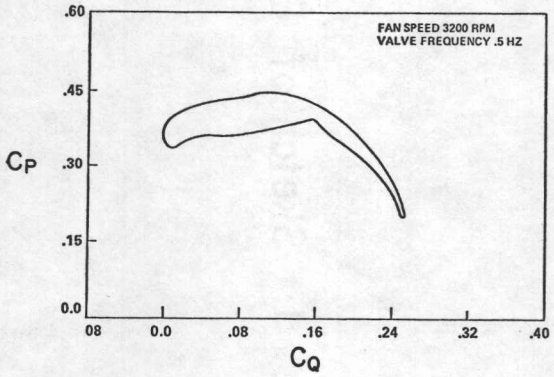

Fig. 2 Typical Results from Reference 1 ω = 0.5 cps

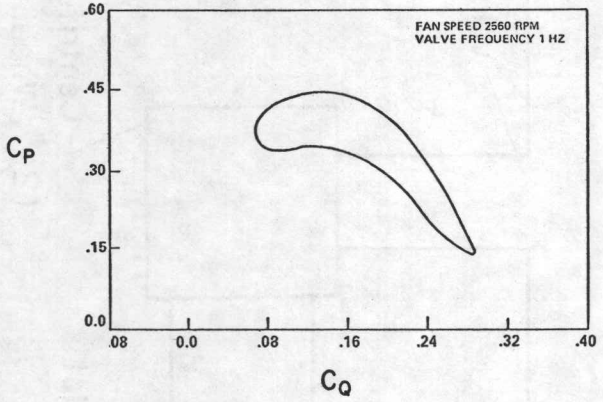

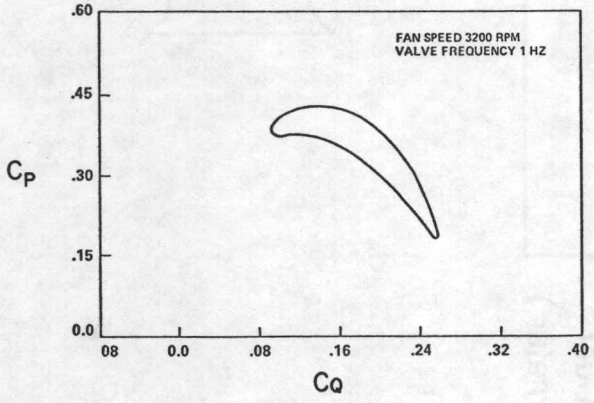

Fig. 3 Typical Results from Ref. 1 ω = 1 cps

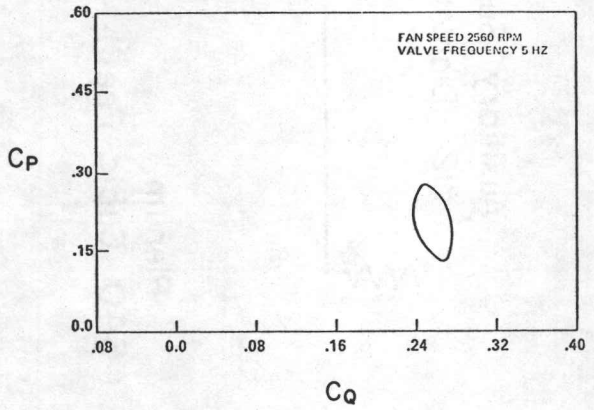

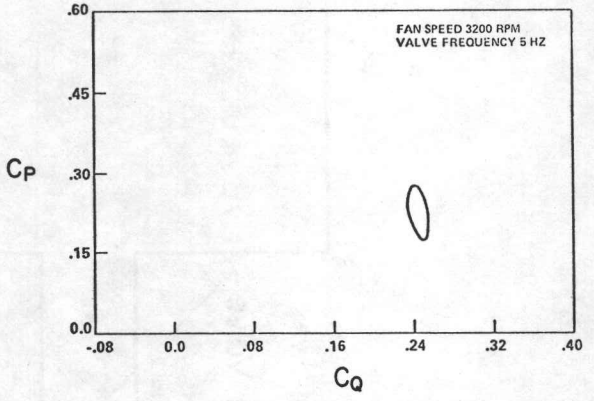

Fig. 4 Typical Results from Ref. 1 ω = 5 cps

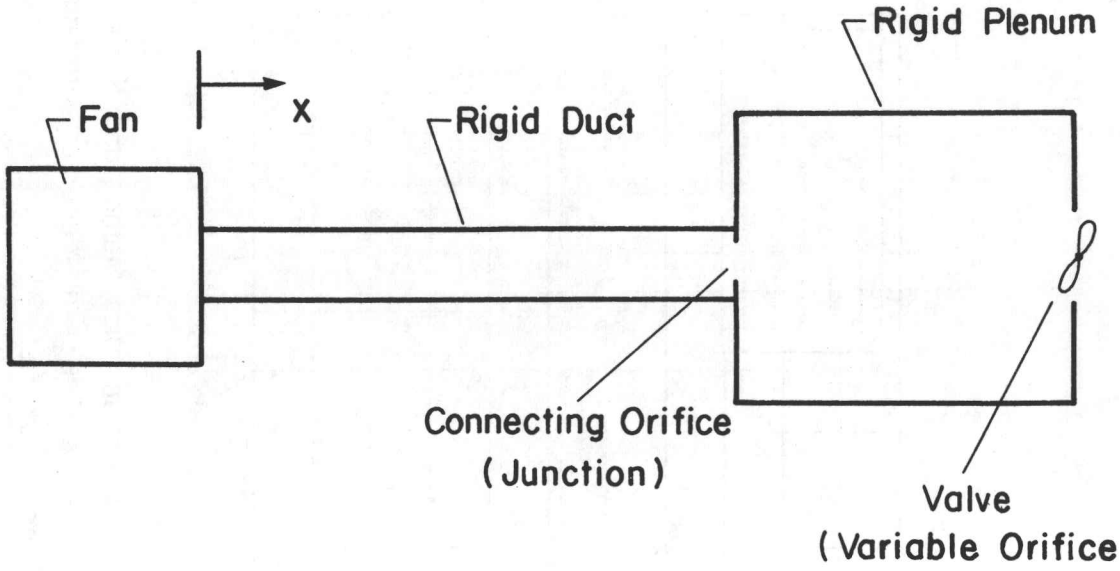

Fig. 5 One Dimensional Model of Fan-Duct-Plenum System.

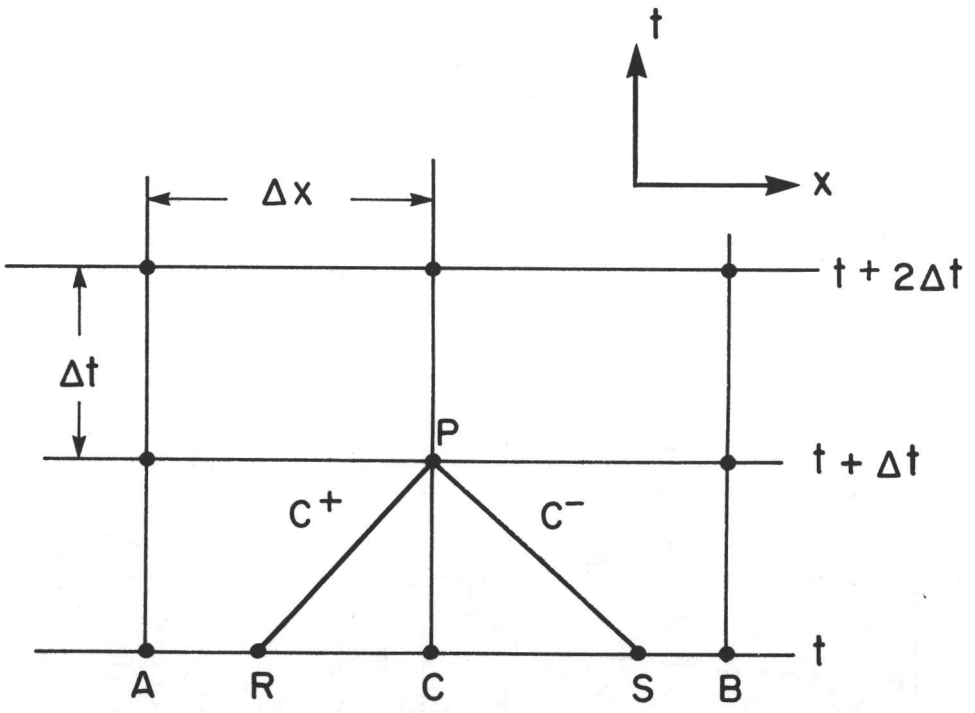

Fig. 6 Characteristic Lines in x-t Plane.

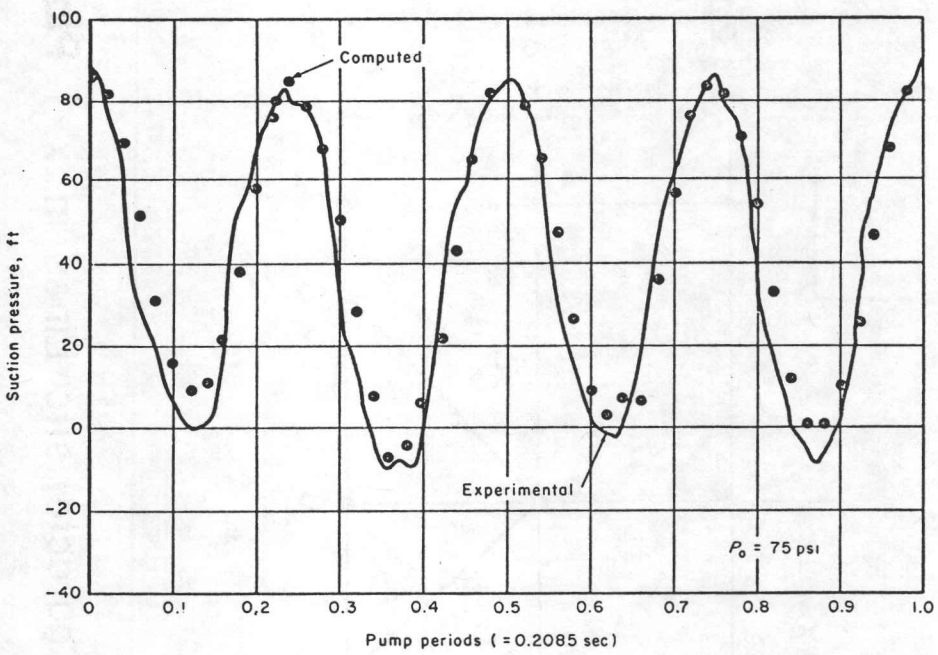

Fig. 7 Comparison of Experimental and Calculated Results for a Single Pipe Connected to a Reciprocating Pump (from Ref. 2)

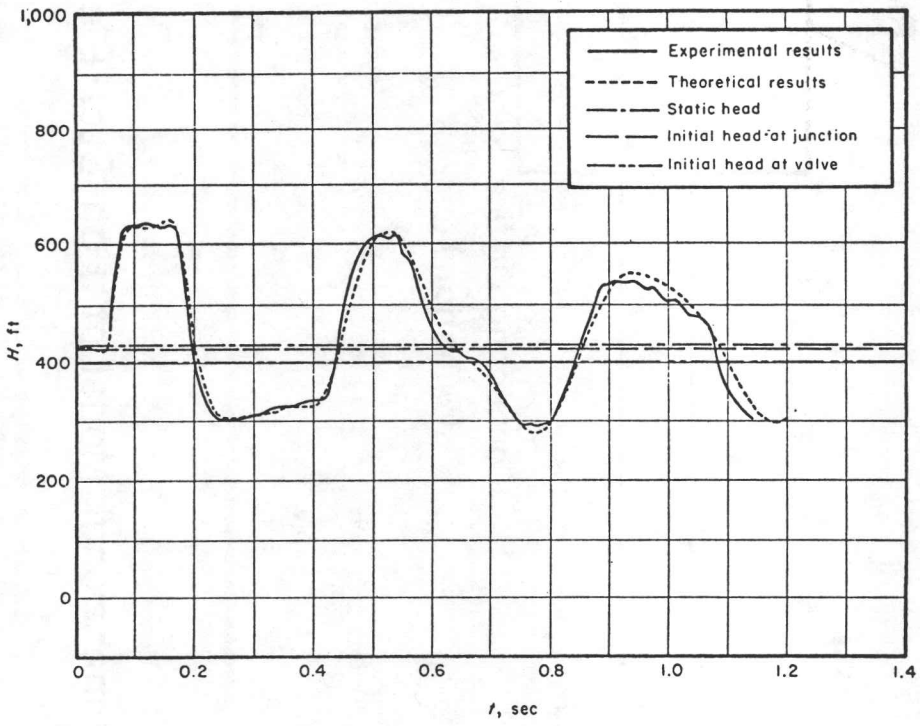

Fig. 8 Comparison of Characteristics Method and Experiment for a Series Pipe-Transducer at Junction Between Pipes. (from Ref. 2)

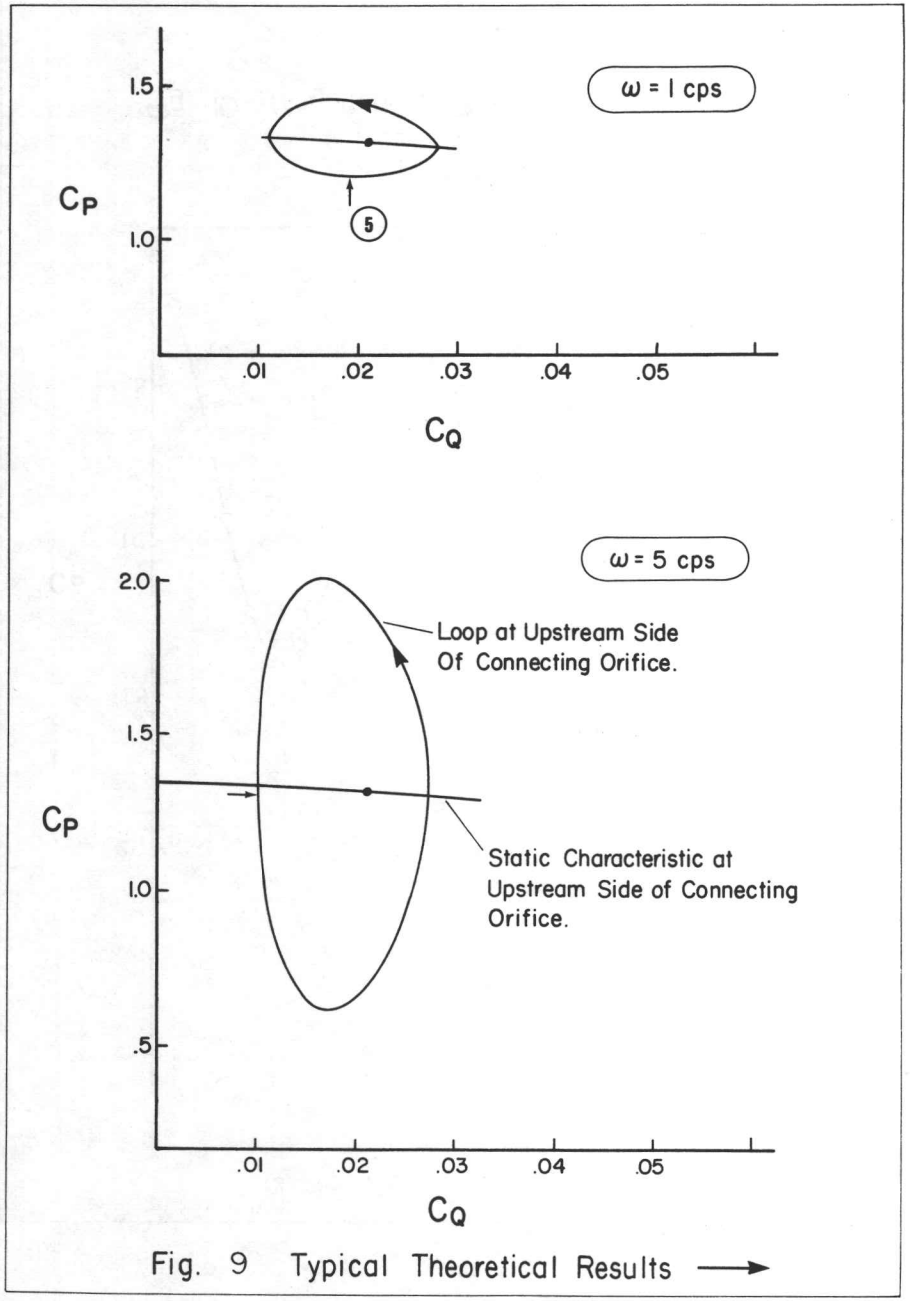

Fig. 9 Typical Theoretical Results →

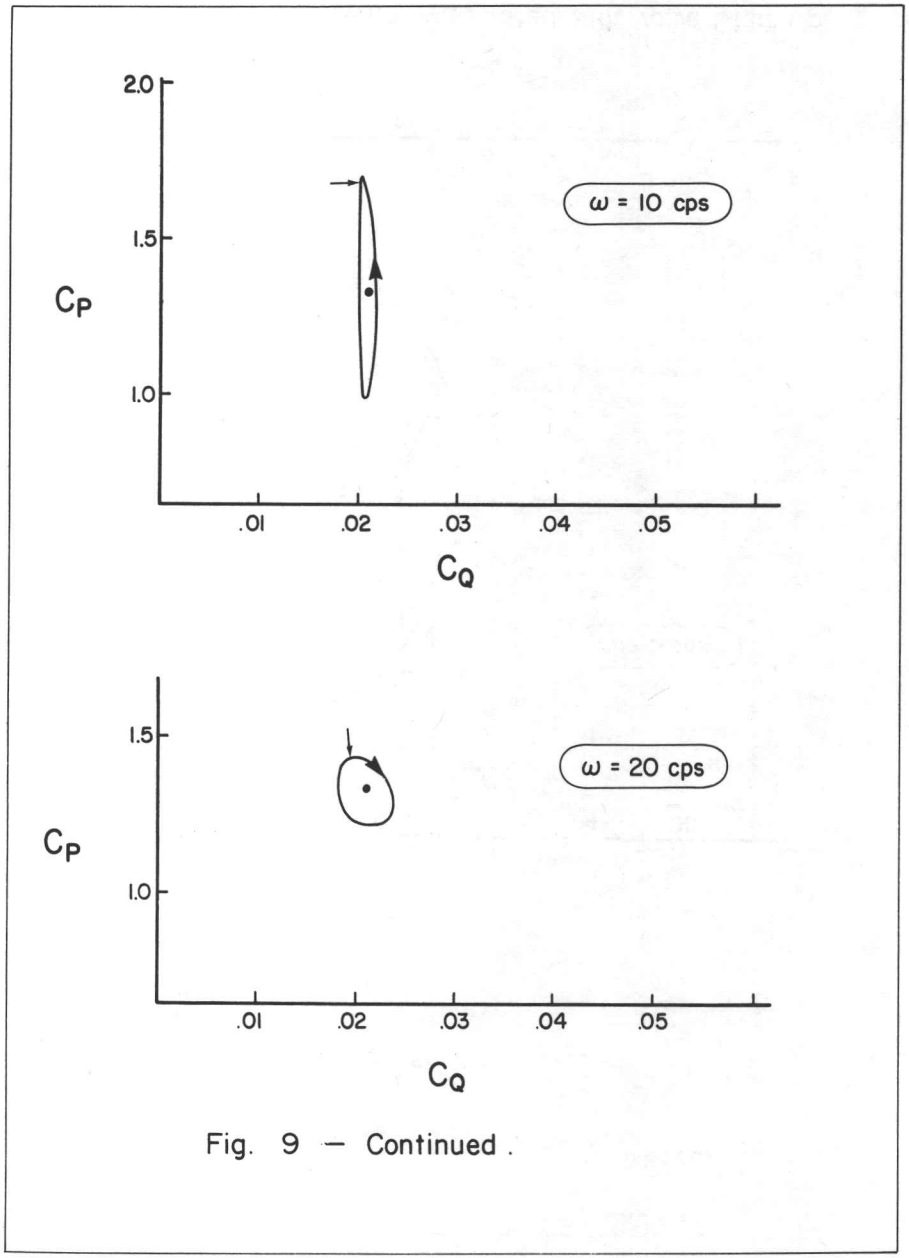

Fig. 9 — Continued .

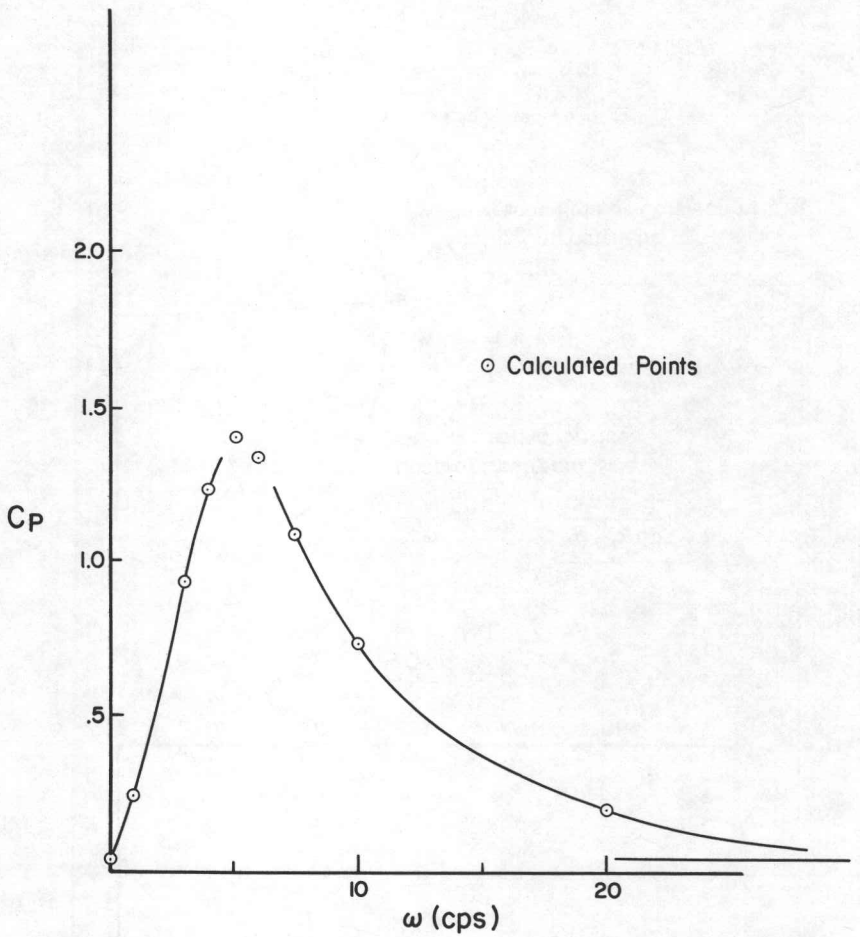

Fig. 10 Magnitude of Pressure Fluctuation vs. Frequency.

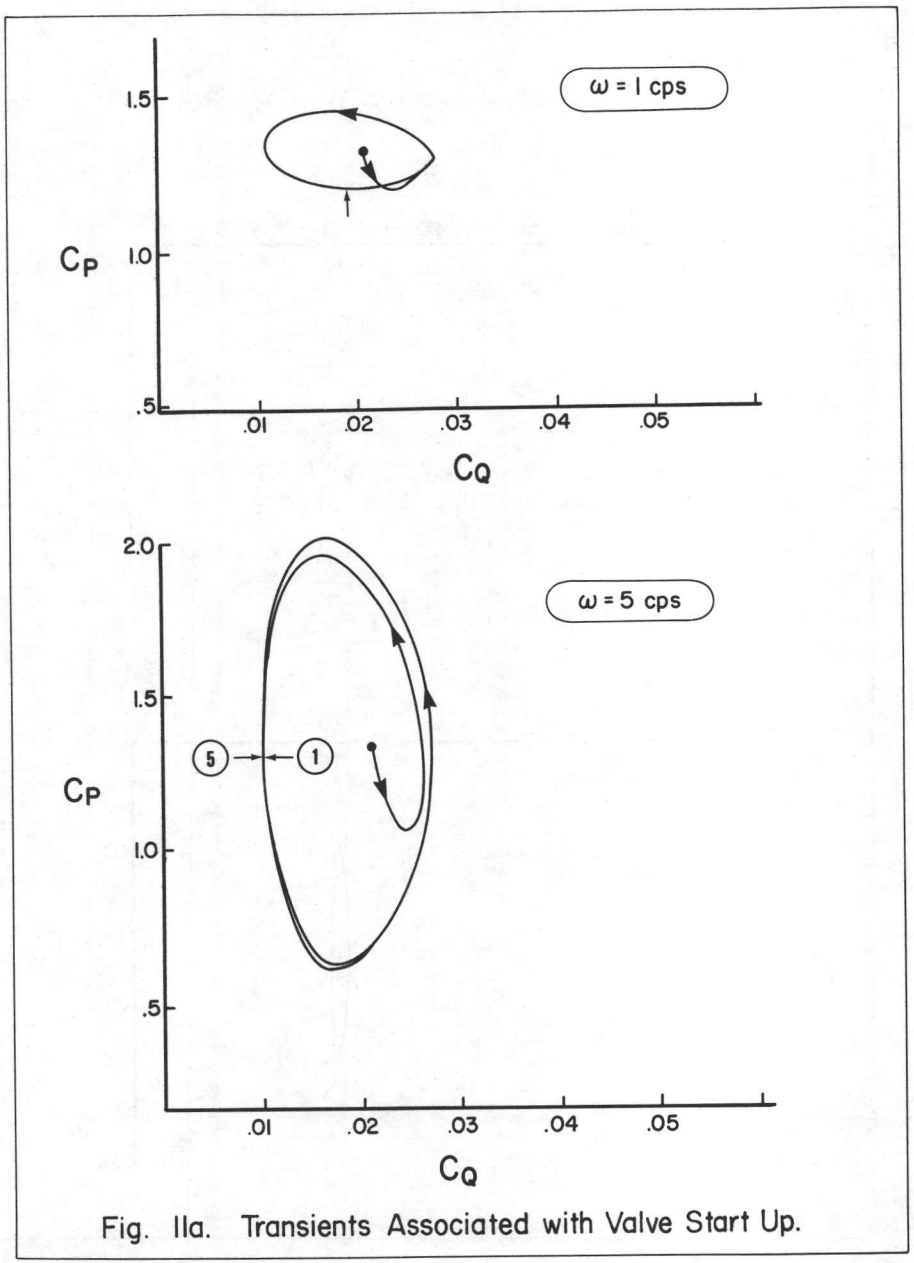

Fig. 11a. Transients Associated with Valve Start Up.

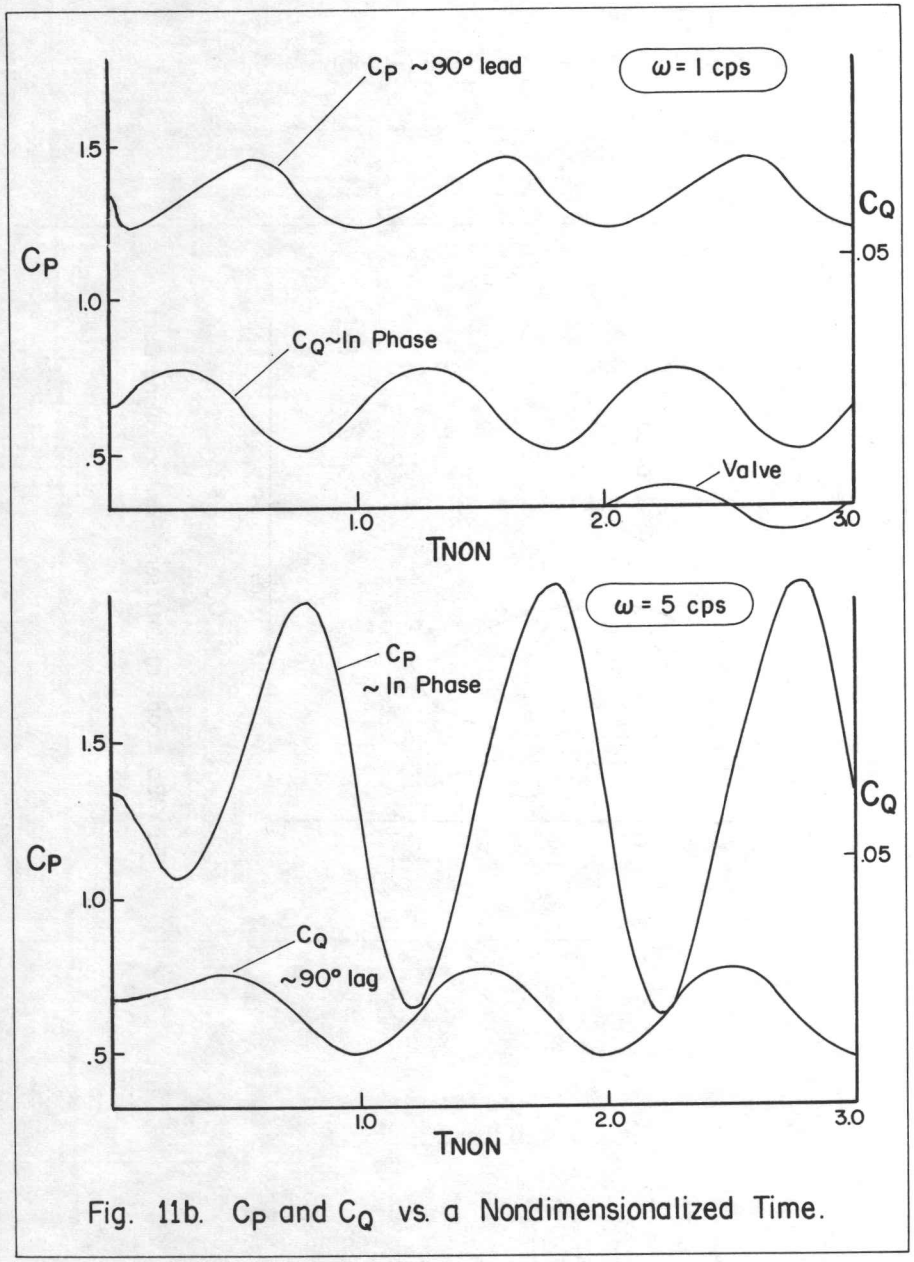

Fig. 11b. C_P and C_Q vs. a Nondimensionalized Time.

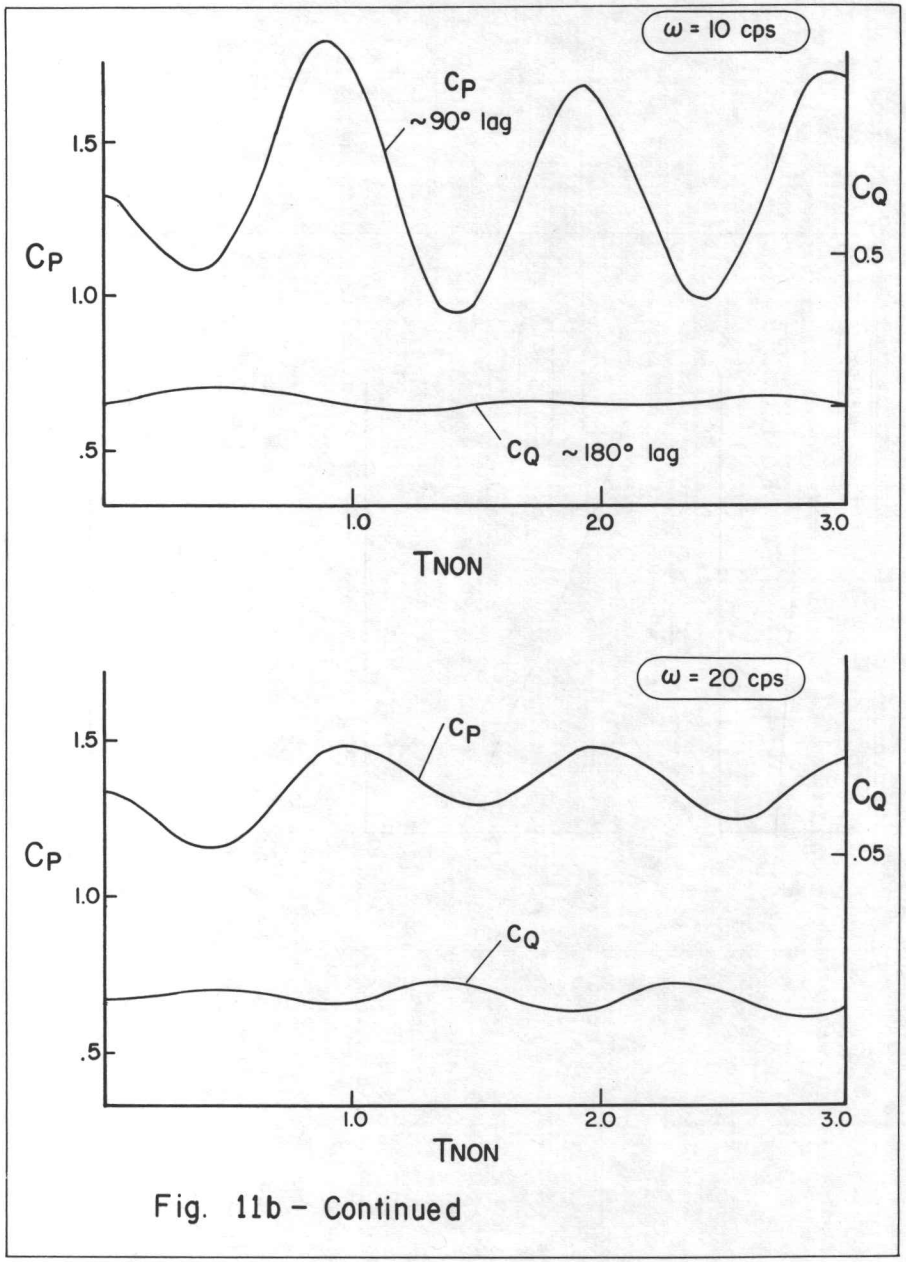

Fig. 11b – Continued

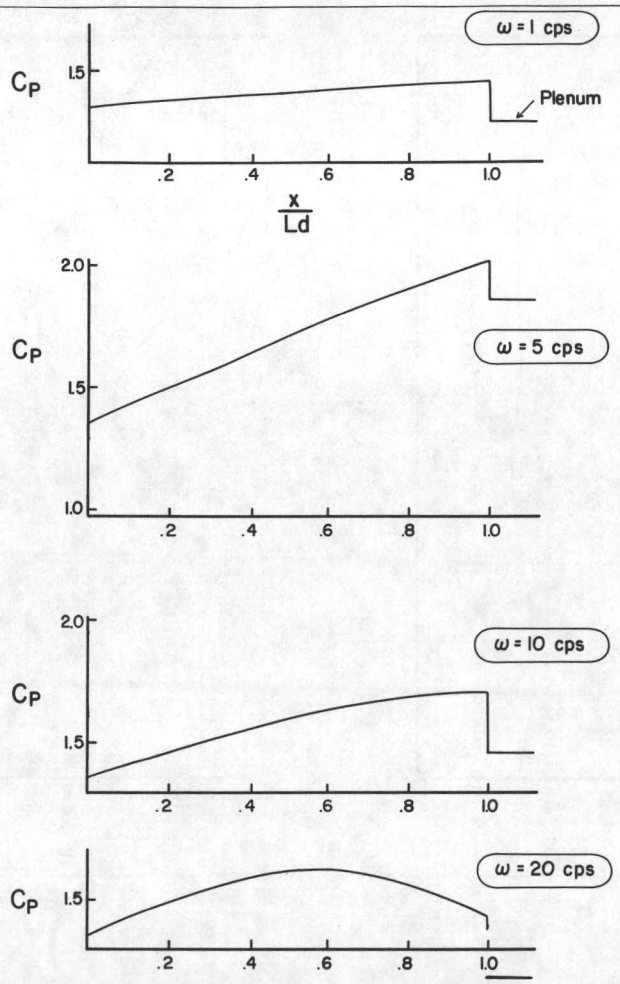

Fig. 12a. Standing Wave Patterns.

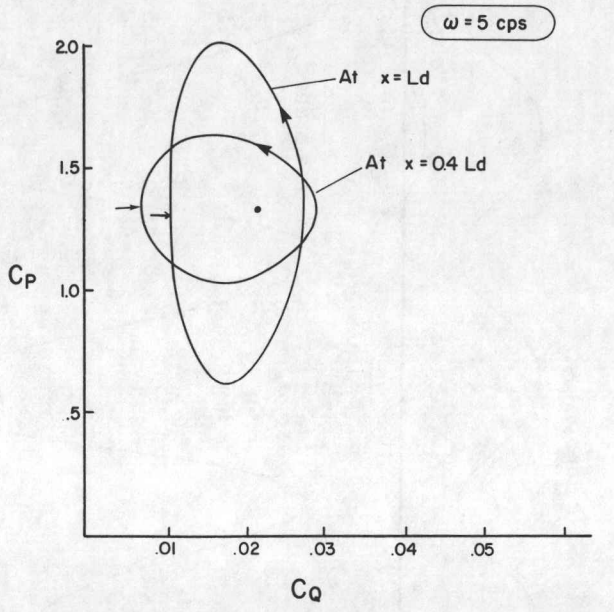

Fig. 12b Loops at Different Positions Along Duct.

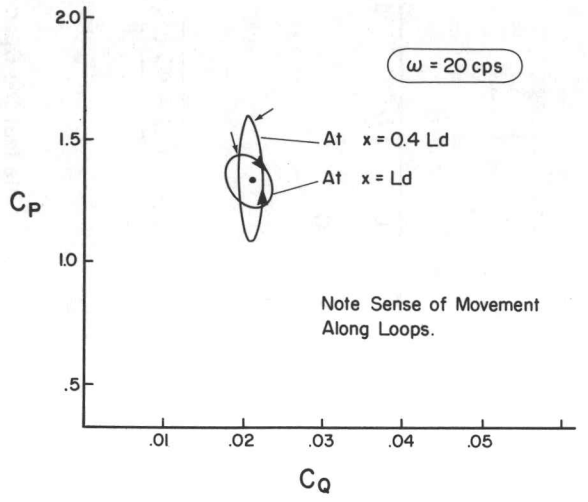

Fig. 12c. Loops at Different Positions Along Duct.

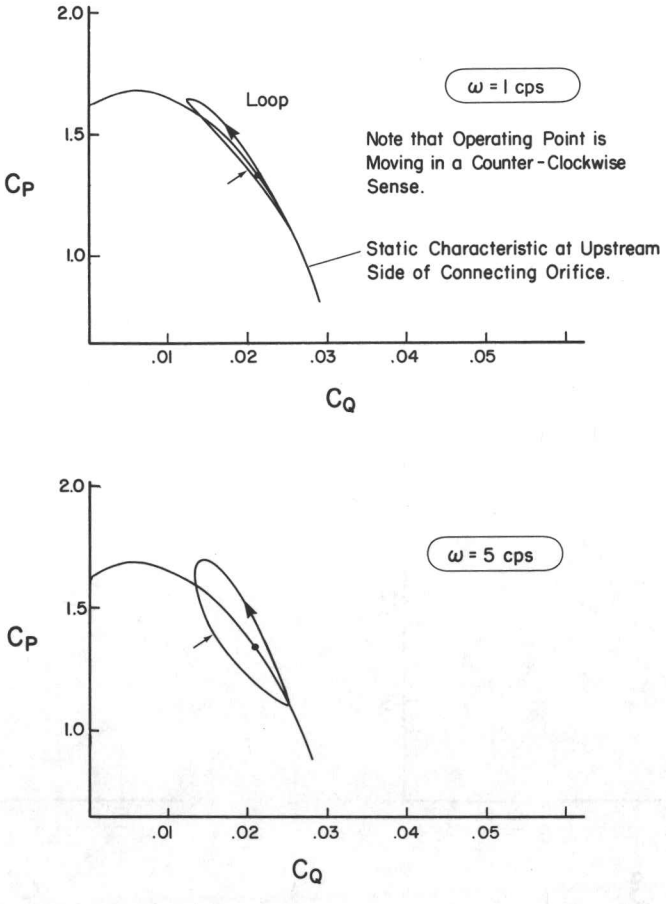

Fig. 13 Short Duct Results

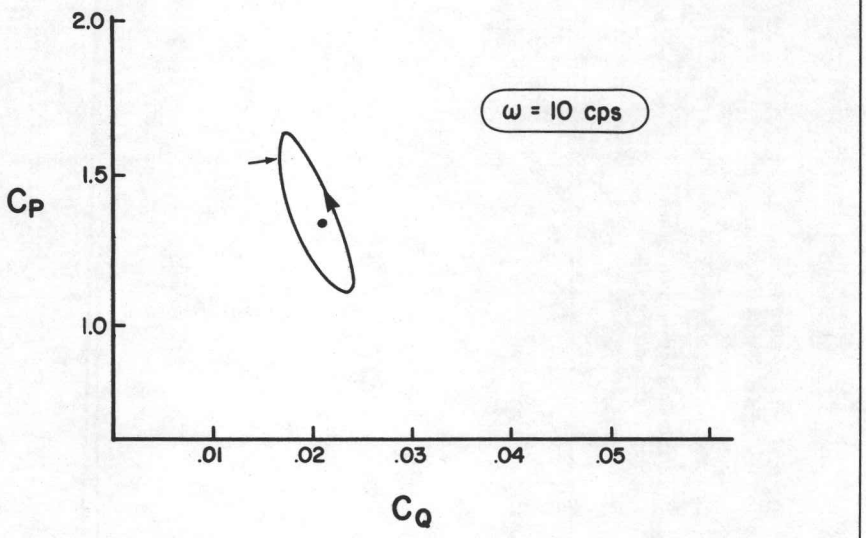

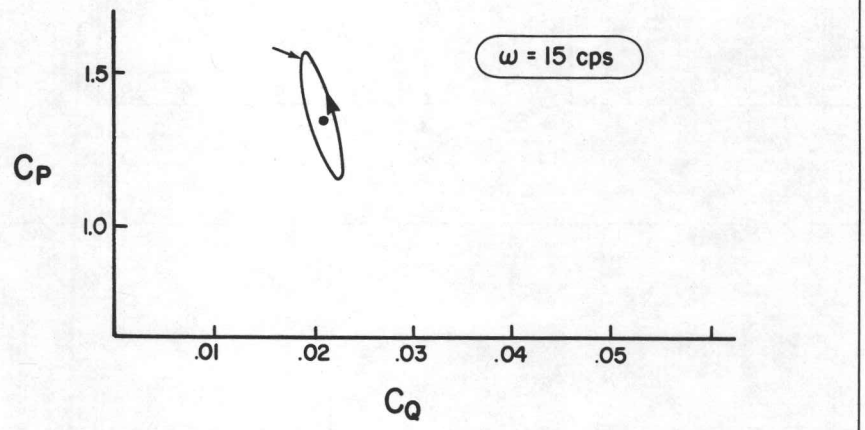

Fig. 13 — Continued.

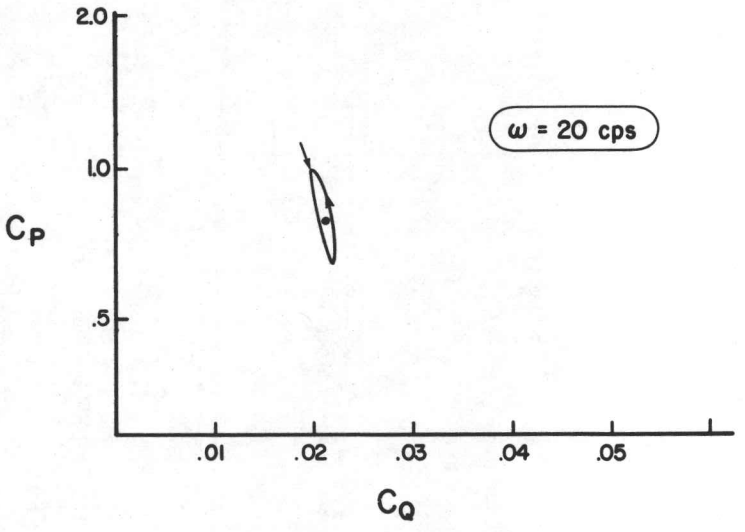

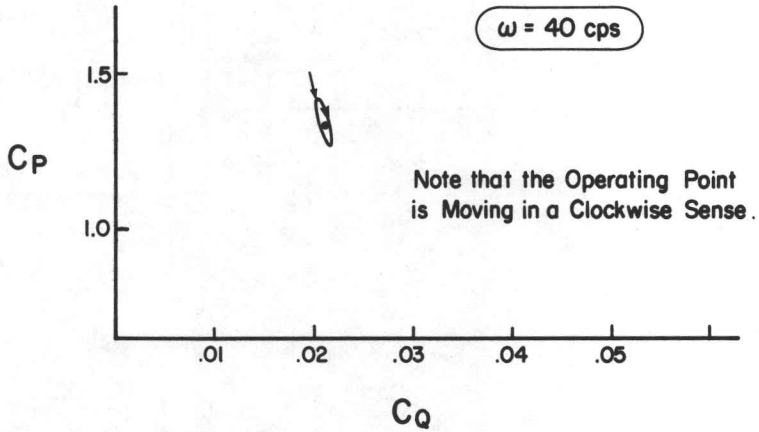

Fig. 13 — Continued.

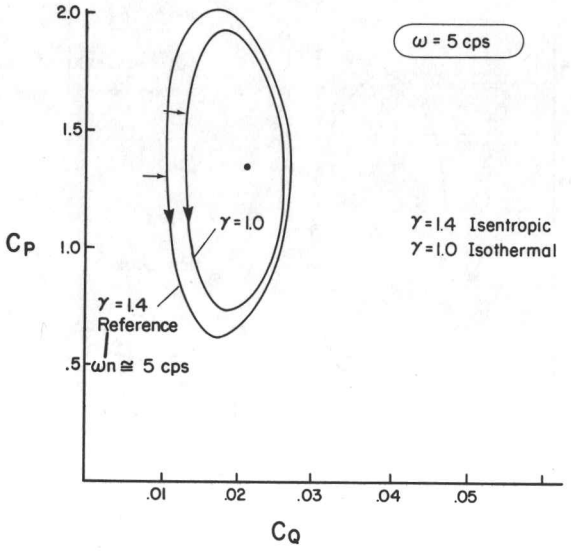

Fig. 14a. Comparison of the Limits of the Polytropic Exponent Approximation.

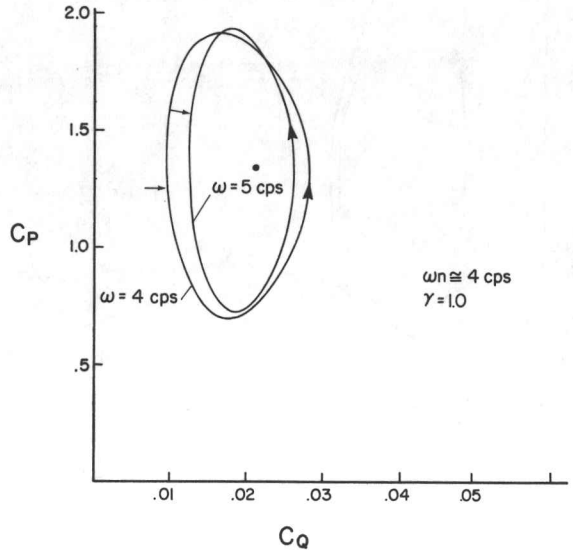

Fig. 14b. Result Showing Change in Natural Frequency.

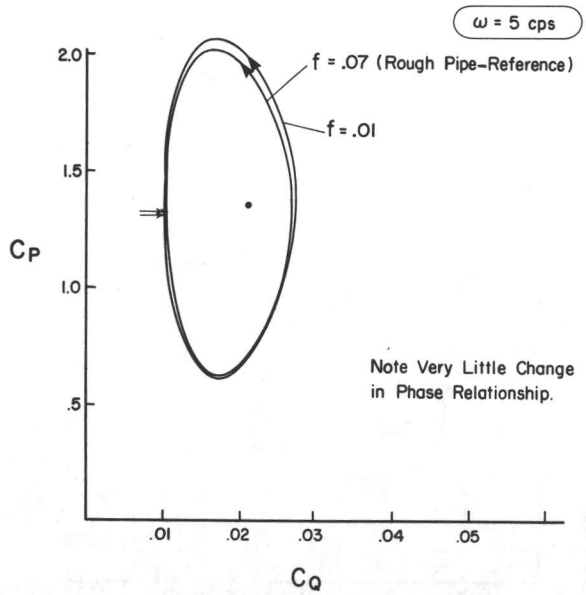

Fig. 15 Friction Factor Effect.

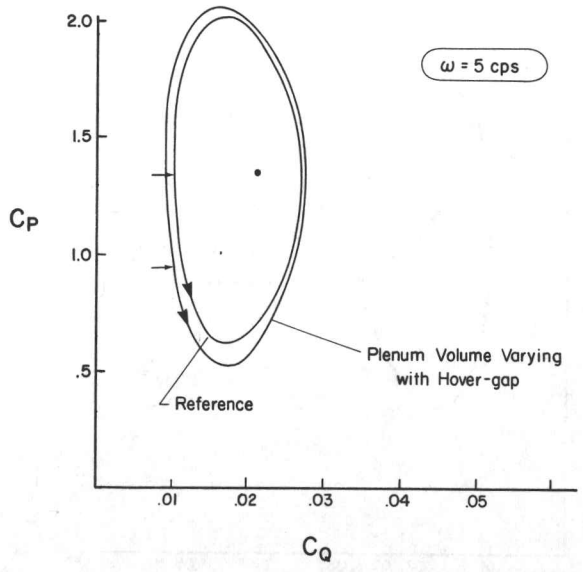

Fig. 16 Result Showing Effect of Plenum Volume Varying with Hover-gap.

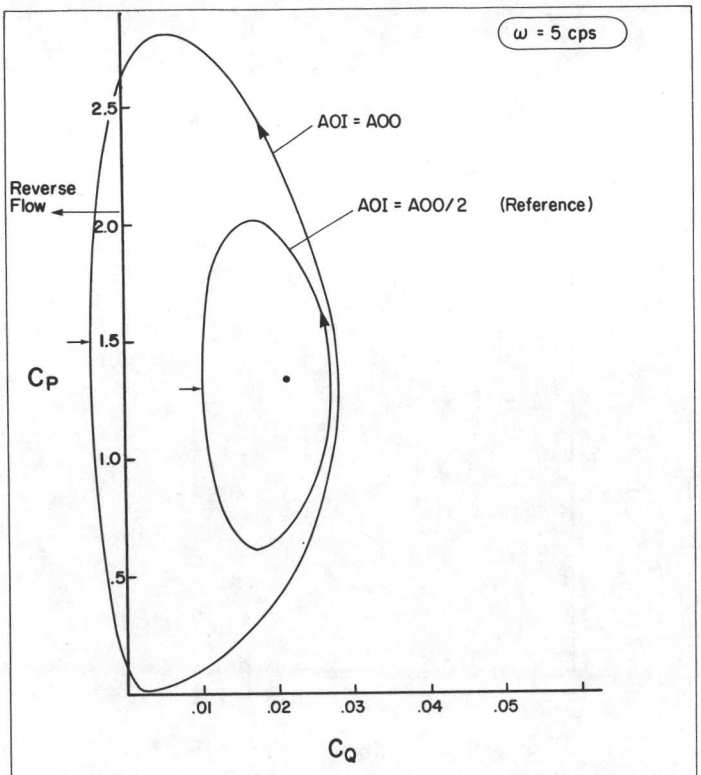

Fig. 17 Result Showing Reverse Flow

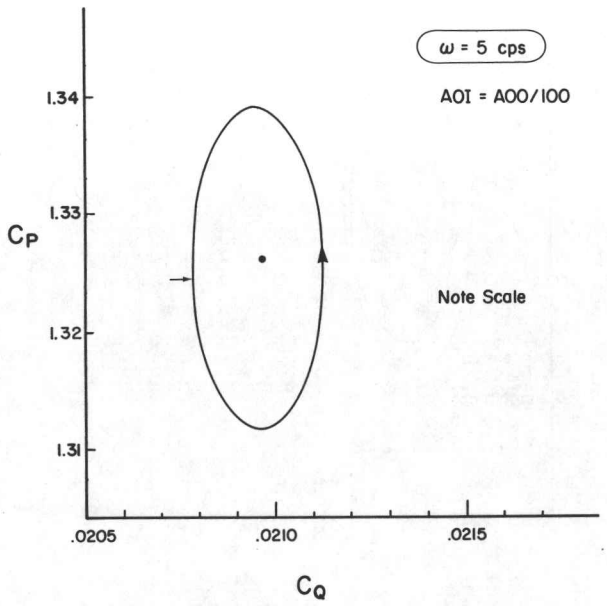

Fig. 18 Result for Very Small Area Variations of Variable Orifice.

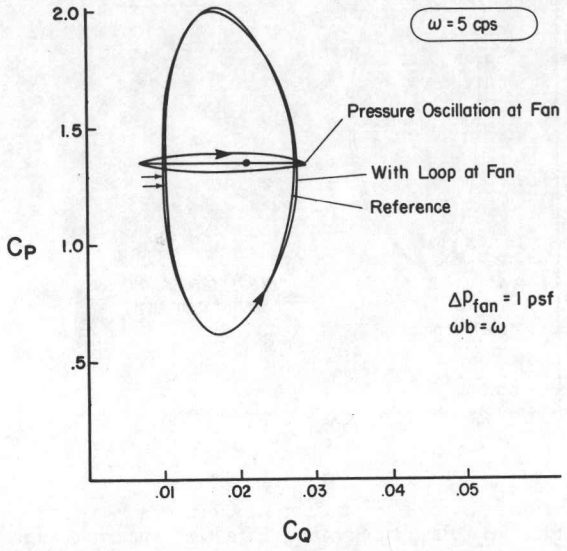

Fig. 19 Typical Result with Loop at Fan.

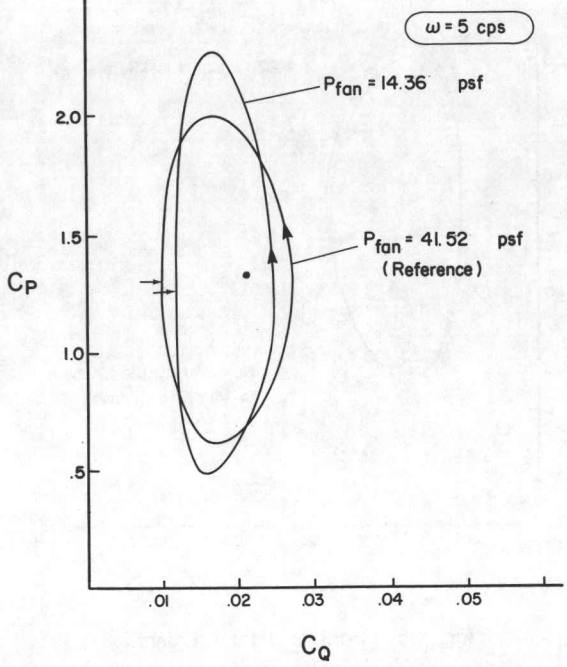

Fig. 20 Result Showing Failure of Fan Scaling Laws.

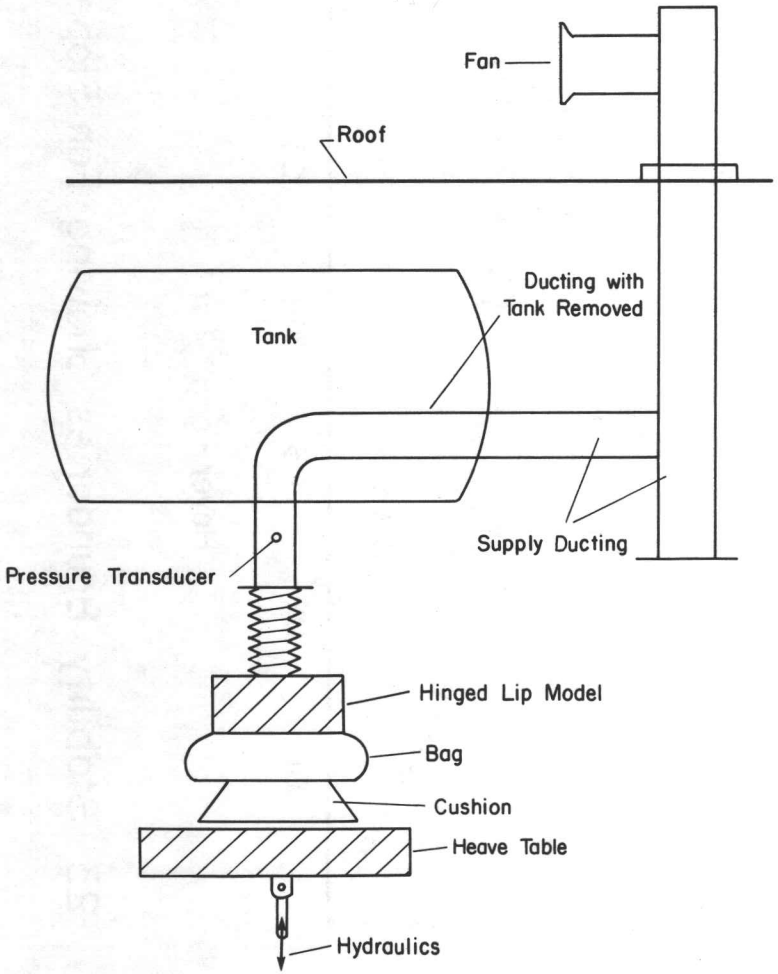

Fig. 21 Heave Table Facility

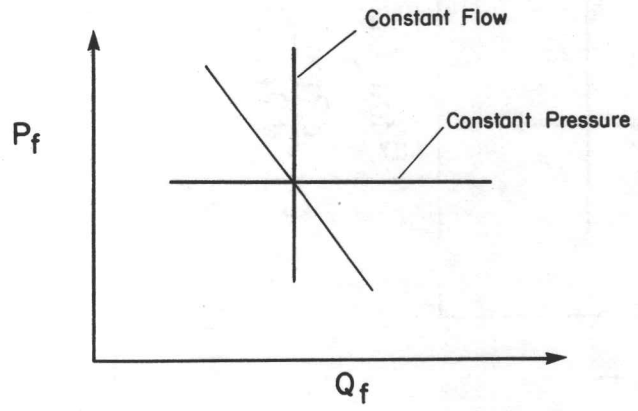

Fig. 22a. Static Characteristics Used in Linear Heave Stability Studies.

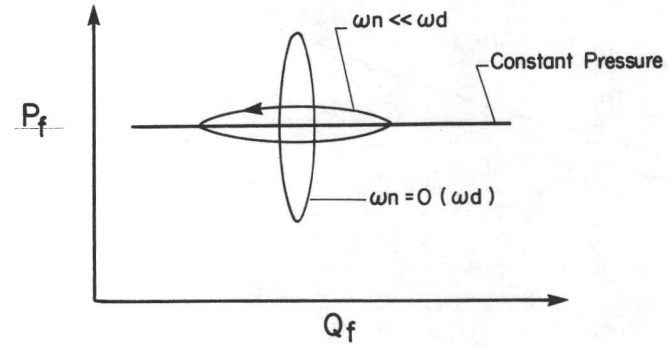

Fig. 22b. Deviation of Dynamic Characteristics from Static Characteristic.

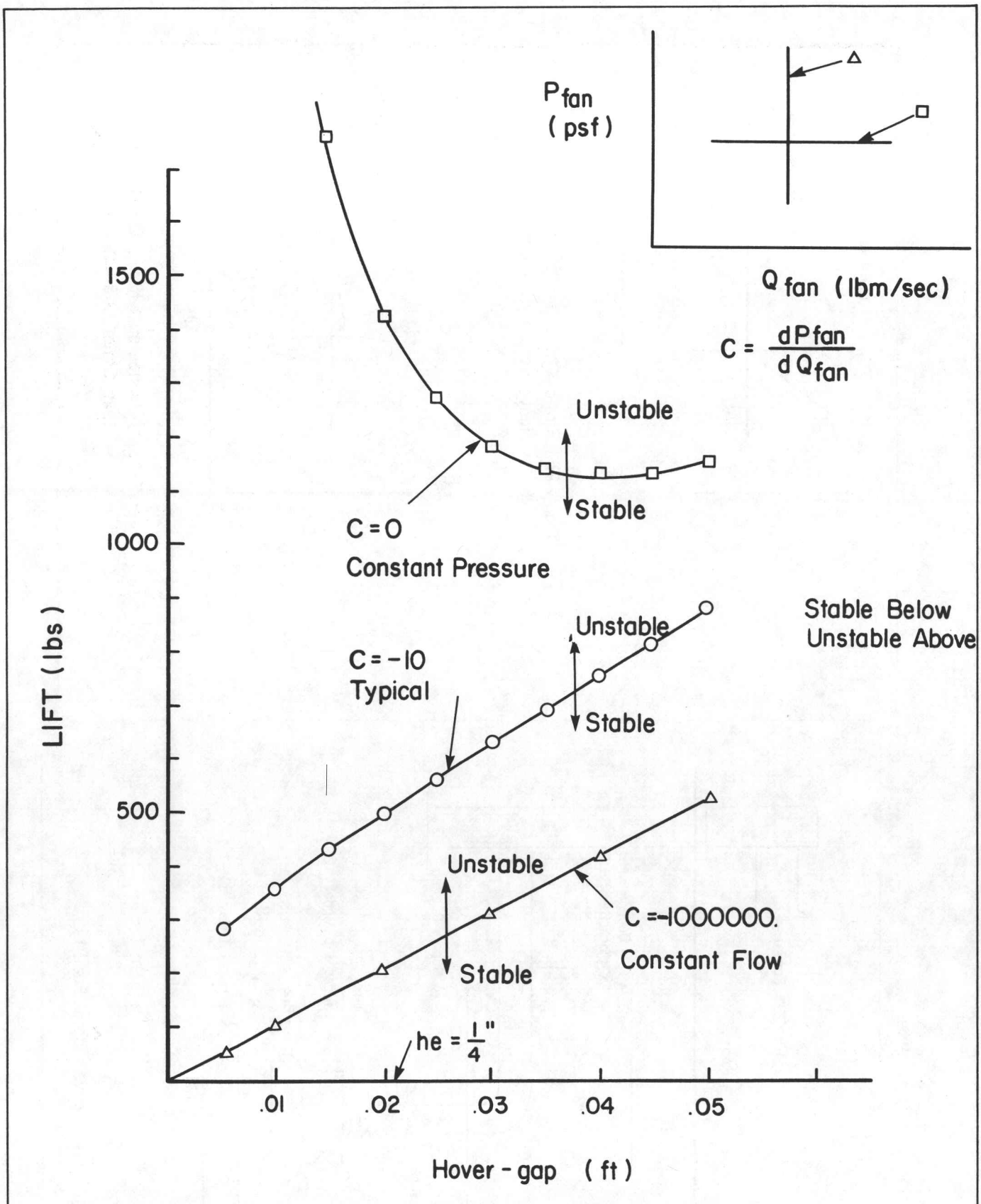

Fig. 23 Stability Boundaries Showing Fan Slope Effect.

APPENDIX A

DETAILS OF THE THEORY

A.1 Governing Equations

The system considered is shown in Fig. A1. It consists essentially of a pipe connected to a plenum by an orifice. For most of the results obtained, the pipe (volute or supply ducting) had a static fan characteristic as its upstream boundary condition. The plenum had a variable orifice (valve) as its downstream boundary condition. The latter boundary condition simulates a varying hover-gap. The analysis is one dimensional in that it assumes that, at any position x along the ducting, conditions are uniform across the cross-section normal to x.

The equations governing the pipe flow are the momentum and continuity equations. Figure A2 shows a typical fluid element within the pipe system. Balancing the pressure, friction, and inertia forces acting on this element, one obtains

$$PA - \left(P + \frac{\partial P}{\partial x} \delta x \right) A - \tau_o \pi D \, \delta x = \rho A \, \delta x \, \dot{V} \qquad (A1)$$

where the various symbols in (A1) are defined in the notation. Equation (A1) reduces to

$$\frac{1}{\rho} \frac{\partial P}{\partial x} + \frac{4\tau_o}{\rho D} + \dot{V} = 0 \qquad (A2)$$

when the pipe is circular, i.e., $A = \pi D^2/4$. Using the Darcy Weisbach expression for the friction stress, i.e.,

$$\tau_o = \frac{\rho f V|V|}{8} \qquad (A3)$$

and the ideal gas relationship, i.e.,

$$\rho = \frac{\bar{P}}{RT} \qquad (A4)$$

Eq. (A2) reduces to

$$\frac{RT}{\bar{P}} \frac{\partial P}{\partial x} + \frac{f V|V|}{2D} + \dot{V} = 0 \qquad (A5)$$

The bar over the P indicates an absolute value. Now, for the results obtained, the maximum pressure variation about the equilibrium (initial) value was approximately 20 psf. The density and temperature variations associated with this pressure variation are less than 1%. Thus, where the density appears as a coefficient, it is possible to assume it to be constant. Here, we let it be equal to its average value, i.e.,

$$\rho_e = \frac{\bar{P}_e}{RT} \qquad (A4)$$

So, Eq. (A5) can be rewritten as

$$\frac{1}{\rho_e}\frac{\partial P}{\partial x} + \frac{f\,V|V|}{2D} + \dot{V} = 0 \tag{A5}$$

$\dot{V}$ is made up of two components, i.e.,

$$\dot{V} = \underbrace{V\frac{\partial V}{\partial x}}_{\text{Convective Term}} + \underbrace{\frac{\partial V}{\partial t}}_{\text{Local Term}} \tag{A6}$$

Thus, with Eq. (A6), Eq. (A5) further reduces to

$$L_1 = \frac{1}{\rho_e}\frac{\partial P}{\partial x} + \frac{f\,V|V|}{2D} + V\frac{\partial V}{\partial x} + \frac{\partial V}{\partial t} = 0 \tag{A7}$$

Continuity requires that the rate of increase of mass of the element must balance with the influx of mass across the element boundary, i.e.,

$$\rho AV - \left(\rho AV + A\frac{\partial}{\partial x}(\rho V)\delta x\right) = \frac{\partial \rho}{\partial t} A\,\delta x \tag{A8}$$

or

$$V\frac{\partial \rho}{\partial x} + \rho_e\frac{\partial V}{\partial x} + \frac{\partial \rho}{\partial t} = 0 \tag{A9}$$

For this, it has been assumed that the pipe is rigid and has a cross-section which does not vary with x. As

$$\dot{\rho} = V\frac{\partial \rho}{\partial x} + \frac{\partial \rho}{\partial t} \tag{A10}$$

Eq. (A9) can be rewritten as

$$\rho_e\frac{\partial V}{\partial x} + \dot{\rho} = 0 \tag{A11}$$

Assuming the compression-expansion processes to behave polytropically, i.e.,

$$\frac{\bar{P}}{\rho^{\gamma}} = K \tag{A12}$$

one can write

$$\dot{\rho} = \frac{1}{a^2}\dot{\bar{P}} = \frac{1}{a^2}\dot{P} \tag{A13}$$

where

$$a = \sqrt{\gamma RT} \tag{A14}$$

is an effective sound speed. With Eq. (A13), Eq. (A11) reduces to

$$L_2 = \frac{\partial V}{\partial x} + \frac{1}{\rho_e a^2}\left(V \frac{\partial P}{\partial x} + \frac{\partial P}{\partial t} \right) = 0 \qquad \text{(A15)}$$

Equations (A7) and (A15) govern the one-dimensional flow of air in a pipe.

A.2 Method of Characteristics

Equations (A7) and (A15) are two coupled quasi-linear hyperbolic partial differential equations. Because of their hyperbolic nature, they can be reduced to four ordinary differential equations by the method of characteristics. The first step in this reduction consists of mutiplying L_2 by λ and adding the result to L_1, i.e.,

$$\begin{aligned} L = L_1 + \lambda L_2 &= 0 \\ &= \left(\frac{1}{\rho_e} \frac{\partial P}{\partial x} + \frac{f\, V|V|}{2D} + V \frac{\partial V}{\partial x} + \frac{\partial V}{\partial t} \right) + \\ &+ \left[\lambda \frac{\partial V}{\partial x} + \lambda \frac{1}{\rho_e a^2} \left(V \frac{\partial P}{\partial x} + \frac{\partial P}{\partial t} \right) \right] \end{aligned} \qquad \text{(A16)}$$

We can rearrange Eq. (A16) to get:

$$(V + \lambda) \frac{\partial V}{\partial x} + \frac{\partial V}{\partial t} + \frac{\lambda}{\rho_e a^2} \left\{ \left(V + \frac{a^2}{\lambda} \right) \frac{\partial P}{\partial x} + \frac{\partial P}{\partial t} \right\} + \frac{f\, V|V|}{2D} = 0 \qquad \text{(A17)}$$

If $P = P(x,t)$ and $V = V(x,t)$ are the solutions of the partial differential equations, then from calculus

$$\frac{dP}{dt} = \frac{\partial P}{\partial x} \frac{dx}{dt} + \frac{\partial P}{\partial t} \qquad \text{(A18.1)}$$

$$\frac{dV}{dt} = \frac{\partial V}{\partial x} \frac{dx}{dt} + \frac{\partial V}{\partial t} \qquad \text{(A18.2)}$$

Thus, if

$$\frac{dx}{dt} = V + \lambda = V + \frac{a^2}{\lambda} \qquad \text{(A19)}$$

which implies $\lambda = \pm a$, then Eq. (A17) becomes

$$\frac{dV}{dt} + \frac{\lambda}{\rho_e a^2} \frac{dP}{dt} + \frac{f\, V|V|}{2D} = 0 \qquad \text{(A20)}$$

Substituting the values of λ into Eqs. (A19) and (A20) gives four ordinary differential equations, i.e.,

$$\left.\begin{aligned} &\frac{dV}{dt} + \frac{1}{\rho_e a}\frac{dP}{dt} + \frac{f\,V|V|}{2D} = 0 && \text{(A21.1)}\\ &\text{on } \frac{dx}{dt} = V + a && \text{(A21.2)}\end{aligned}\right\} C^+$$

$$\left.\begin{aligned} &\frac{dV}{dt} - \frac{1}{\rho_e a}\frac{dP}{dt} + \frac{f\,V|V|}{2D} = 0 && \text{(A21.3)}\\ &\text{on } \frac{dx}{dt} = V - a && \text{(A21.4)}\end{aligned}\right\} C^-$$

The solutions of Eqs. (A21.2) and (A21.4) give the characteristic lines in the x-t plane along which disturbances given by Eqs. (A21.1) and (A21.3) propagate.

A.3 Solution of the Ordinary Differential Equations

The ordinary differential equations can be solved numerically by a first-order finite difference technique known as the method of specified time intervals. This technique is basically just a simple Euler integration. The finite difference forms of the equations are (see Fig. A3):

$$V_P - V_R + \frac{1}{\rho_{R_e}}\frac{(P_P - P_R)}{a} + \frac{f}{2D}V_R|V_R|(t_P - t_R) = 0 \qquad \text{(A22.1)}$$

$$x_P - x_R = (V_R + a)(t_P - t_R) \qquad \text{(A22.2)}$$

$$V_P - V_S - \frac{1}{\rho_{S_e}}\frac{(P_P - P_S)}{a} + \frac{f}{2D}V_S|V_S|(t_P - t_S) = 0 \qquad \text{(A22.3)}$$

$$x_P - x_S = (V_S - a)(t_P - t_S) \qquad \text{(A22.4)}$$

where $\Delta t = t_P - t_R = t_P - t_S$. To be able to solve for conditions at position P in the x-t plane, conditions at positions R and S must be known. With Δx and Δt specified and with known conditions at A, B, and C, one can obtain conditions at R and S by linear interpolation. For example,

$$\frac{x_P - x_R}{\Delta x} = \frac{V_C - V_R}{V_C - V_A} \qquad \text{(A23)}$$

Using Eq. (A22.2), Eq. (A23) becomes

$$\frac{(V_R + a)\Delta t}{\Delta x} = \frac{V_C - V_R}{V_C - V_A} \tag{A24}$$

or

$$(V_R + a)\theta = \frac{V_C - V_R}{V_C - V_A} \tag{A25}$$

where $\theta = \Delta t/\Delta x$. Solving for V_R, one obtains

$$V_R = \frac{V_C - (V_C - V_A)a\theta}{1 + \theta(V_C - V_A)} \tag{A26}$$

Similarly

$$V_S = \frac{V_C - (V_C - V_B)a\theta}{1 - \theta(V_C - V_B)} \tag{A27}$$

and

$$P_R = P_C - \theta(V_R + a)(P_C - P_A) \tag{A28}$$

$$P_S = P_C + \theta(V_S - a)(P_C - P_B) \tag{A29}$$

To simplify the solution of equations (A22.1) and (A22.3) for V_P and P_P, we let $\rho_{R_e} = \rho_{S_e} = \rho_{C_e}$ and finally get

$$V_P = \frac{1}{2}\left\{ V_R + V_S + \frac{1}{\rho_{C_e}} \frac{(P_R - P_S)}{a} - \frac{f}{2D} \Delta t(V_R|V_R| + V_S|V_S|) \right\} \tag{A30}$$

$$P_P = \frac{1}{2}\left\{ P_R + P_S + \rho_{C_e} a\,(V_R - V_S) - \rho_{C_e} \frac{fa}{2D} \Delta t(V_R|V_R| - V_S|V_S|) \right\} \tag{A31}$$

For stability and convergence of the finite difference scheme, Δt must be less than Δx divided by $(V + a)$.

A.4 Boundary Conditions

Fan

For most of the results obtained, a static fan characteristic of the form

$$P_{fan} = C_o + C_1 V_{fan} + C_2 V_{fan}^2 \tag{A32}$$

was used as the fan boundary condition. Effectively, this condition was imposed immediately downstream of the fan blades. To be able to solve for P_{fan} and V_{fan} at time $t + \Delta t$, one other equation relating these two unknowns is required. The equation available here is the C^- characteristic equation, i.e. (see Fig. A4),

$$V_{fan} - V_S - \frac{1}{\rho_{Se}} \frac{(P_{fan} - P_S)}{a} + \frac{f}{2D} V_S |V_S| (t_{fan} - t_S) = 0 \qquad (A33)$$

where as before

$$V_S = \frac{V_C - (V_C - V_B)a\theta}{1 - \theta(V_C - V_B)} \qquad (A27)$$

and

$$P_S = P_C + \theta(V_S - a)(P_C - P_B) \qquad (A28)$$

We can solve Eq. (A33) for P_{fan} in terms of V_{fan} and substitute into Eq. (A32) to get a quadratic in V_{fan}. Solving the quadratic in the usual manner gives V_{fan} and thus P_{fan}. For more general characteristics, such a procedure will not work. Instead, an iterative procedure such as the Newton Raphson iteration must be employed. Here, we illustrate this procedure by applying it to Eqs. (A32) and (A33). For this, the equations must be put into the form $F_i = 0$, i.e.,

$$F_1 = P_{fan} - C_o - C_1 V_{fan} - C_2 V_{fan}^2 = 0 \qquad (A34)$$

$$F_2 = V_{fan} - V_S - \frac{1}{\rho_{Se}} \frac{(P_{fan} - P_S)}{a} + \frac{f}{2D} V_S |V_S| (t_{fan} - t_S) = 0 \qquad (A35)$$

The derivatives of these two equations with respect to the unknowns P_{fan} and V_{fan} are

$$\begin{aligned} a_{11} &= \frac{\partial F_1}{\partial P_{fan}} = 1 \\ a_{12} &= \frac{\partial F_1}{\partial V_{fan}} = - C_1 - 2C_2 V_{fan} \\ a_{21} &= \frac{\partial F_2}{\partial P_{fan}} = - \frac{1}{\rho_{Se} a} \\ a_{22} &= \frac{\partial F_2}{\partial V_{fan}} = 1 \end{aligned} \qquad (A36)$$

The derivatives are elements of the Jacobian matrix, J, i.e.,

$$J = \begin{vmatrix} a_{11} & a_{12} \\ a_{21} & a_{22} \end{vmatrix} \qquad (A37)$$

The inverse Jacobian matrix is

$$\begin{vmatrix} A_{11} & A_{12} \\ A_{21} & A_{22} \end{vmatrix} \tag{A38}$$

where

$$A_{11} = \frac{a_{22}}{Det} \qquad A_{12} = \frac{-a_{12}}{Det}$$

$$A_{21} = \frac{-a_{21}}{Det} \qquad A_{22} = \frac{a_{11}}{Det} \tag{A39}$$

where Det is the determinant of the Jacobian matrix, i.e.,

$$Det = a_{11}\, a_{22} - a_{21}\, a_{12} \tag{A40}$$

The Newton Raphson iteration formulae are

$$P_{fan_{i+1}} = P_{fan_i} - (A_{11}\, F_1 + A_{12}\, F_2)_i \tag{A41}$$

$$V_{fan_{i+1}} = V_{fan_i} - (A_{21}\, F_1 + A_{22}\, F_2)_i \tag{A42}$$

In some of the results obtained, a blade passing frequency effect was simulated by replacing Eq. (A32) by

$$P_{fan} = \overline{P_{fan}} + \Delta P_{fan}\, Sin(2\pi\, \omega_b\, t) \tag{A32}$$

$\overline{P_{fan}}$ is the equilibrium or mean value of the fan pressure. ω_b is the blade passing frequency. The boundary condition imposes at the fan a small sinusoidal pressure disturbance. We assume the pressure disturbance is associated with a blade passing frequency effect. With P_{fan} known as a function of time, V_{fan} can be obtained directly from the C^- characteristic equation.

Connecting Orifice

For this case, the unknowns are P_{co} and V_{co}. These are respectively the pressure and the velocity immediately upstream of the connecting orifice at time $t + \Delta t$. As a boundary condition, we use the quasi-steady, inviscid incompressible, orifice flow equation

$$V_{co}\, A_d = C_d\, A_{co} \sqrt{\frac{2(P_{co} - P_c)}{\rho_e}} \tag{A43}$$

This reduces to

$$C_{co}(P_{co} - P_c) - V_{co}|V_{co}| = 0 \tag{A44}$$

where

$$C_{co} = \frac{C_d^2 A_{co}^2}{A_d^2} \frac{2}{\rho_e} \tag{A45}$$

For P_c, we use its value at time t. Now, as before, we require one other equation relating P_{co} and V_{co}. The equation available here is the C^+ characteristic equation, i.e.,

$$V_{co} - V_R + \frac{1}{\rho_{R_e}} \frac{(P_{co} - P_R)}{a} + \frac{f V_R |V_R|}{2D} \tag{A46}$$

where V_R and P_R are known interpolated values at time t. Again, we can solve (A46) for P_{co} in terms of V_{co} and substitute into (A44) to get a quadratic in V_{co}. Alternatively, we could use a Newton Raphson iteration. In the computer program, a Newton Raphson iteration is used.

A.5 Lumped Parameter Equations for a Rigid Plenum

For a plenum which is fixed in the inertial reference frame, there is basically only one lumped parameter equation. This equation was derived in Appendix A of Ref. 5 and is basically just a statement of conservation of mass, i.e.,

$$\frac{dP_c}{dt} = \frac{(Q_c - Q_a)}{\forall_c} \rho_e a^2 - \frac{\overline{P_c} \gamma S_a}{\forall_c} \frac{dh}{dt} \tag{A47}$$

where

$$\forall_c = \forall_o + S_b h \qquad = \text{Plenum Volume} \tag{A48}$$

$$Q_c = C_d A_{co} \sqrt{\frac{2(P_{co} - P_c)}{\rho_e}} \qquad = \text{Plenum Inflow} \tag{A49}$$

$$Q_a = C_d A_o \sqrt{\frac{2P_c}{\rho_e}} \qquad = \text{Plenum Outflow} \tag{A50}$$

where

$$A_o = A_{o\mp} \sin(2\pi \omega t) + A_{oo} \tag{A51}$$

or

$$\ell_P h = \ell_P \Delta h \sin(2\pi \omega t) + \ell_P h_e \tag{A52}$$

In the computer program, Eq. (A47) is integrated numerically by a fourth order Runge Kutta procedure. The time step for this integration is fixed and is the same as that used for the duct integrations.

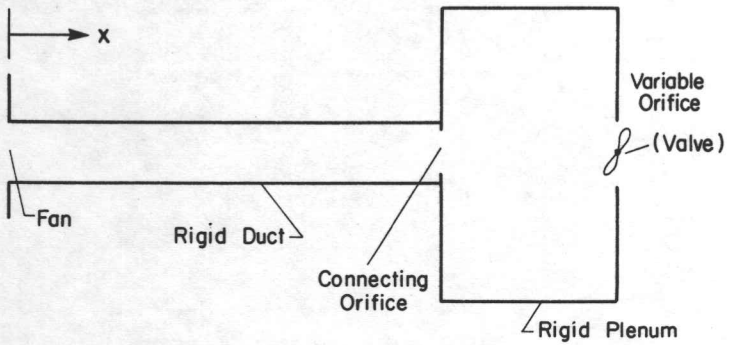

Fig. A1 System Model

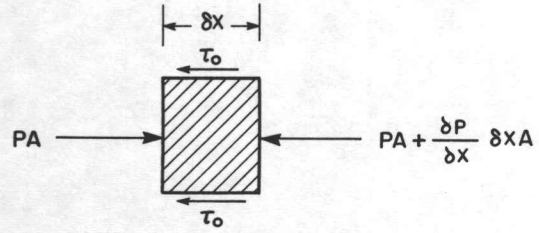

Fig. A2 Typical Fluid Element

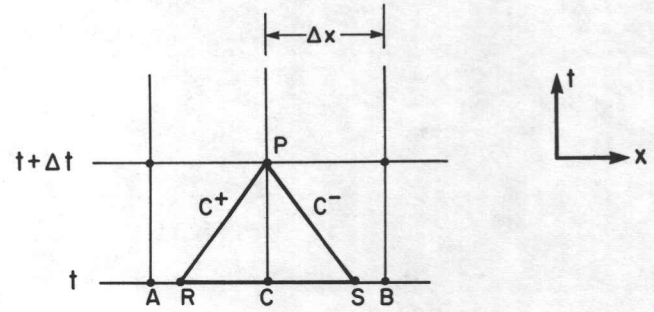

Fig. A3 Characteristic Lines in x-t Plane.

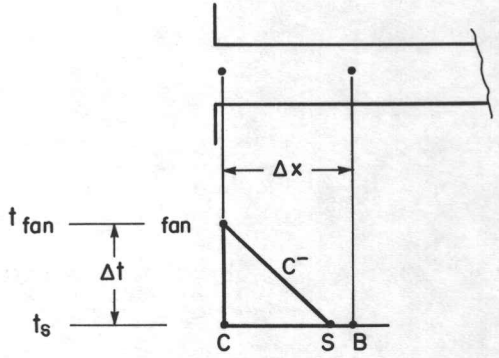

Fig. A4 Fan Boundary Condition.

APPENDIX B. COMPUTER PROGRAM LISTING

```
$JOBRL


C
C
C     DYNAMIC FAN CHARACTERISTICS OF AIR CUSHION SYSTEMS.
C     BY THE METHOD OF CHARACTERISTICS.
C
C
      IMPLICIT REAL*8(A-H,O-Z)
      DIMENSION P(90),PP(90),VP(90),VV(90)
      DIMENSION PN(90),QN(90)
      DIMENSION AA(4,4),FF(4),XF(4),LL(4),M(4)
      REAL L1,L2,N,KP,NR
C
C     T........TIME.
C     NO.......NUMBER OF DUCT NODES.
C     DELX.....X DISCRETIZATION.
C     DELT.....TIME DISCRETIZATION.
C     D1.......DUCT DIAMETER.
C     D2.......PLENUM DIAMETER.
C     L1.......DUCT LENGTH.
C     L2.......PLENUM LENGTH.
C     SP.......SOUND SPEED.
C     FR.......FRICTION FACTOR.
C     CD.......DISCHARGE COEFFICIENT.
C     PHI......3.14159
C     G........GRAVITATIONAL ACCELERATION.
C     R........GAS CONSTANT FOR AIR.
C     TR.......AIR TEMPERATURE.
C     KP.......POLYTROPIC EXPONENT.
C     ROW......AIR DENSITY.
C     PO,C1,C2 FAN COEFFICIENTS.
C     FSP......FAN SPEED.
C     FDIA.....FAN DIAMETER.
C     AFO......AREA OF CONNECTING ORIFICE.
C     AO.......EXIT AREA FROM PLENUM.
C     AP.......DUCT CROSS-SECTIONAL AREA.
C     SA.......PLENUM CROSS SECTIONAL AREA.
C     CP.......PLENUM PERIMETER AT GROUND LEVEL.
C     QC.......FLOW INTO PLENUM.
C     QA.......FLOW OUT OF PLENUM.
C     VC.......PLENUM VOLUME.
C     HE.......EQUILIBRIUM HOVER GAP.
C     H........HOVER GAP.
C     ZO.......AMPLITUDE OF HOVER GAP VARIATION.
C     W........CIRCULAR FREQUENCY OF HOVER GAP VARIATION.
C
C
C     DATA.
      READ(5,100) L1,L2,N,AP,SA
  100 FORMAT(5F10.3)
      READ(5,101) G,R,TR,KP,FR,FSP,FDIA
      READ(5,101) CD,ROW,PHI,PO,C1,C2,VMAX
  101 FORMAT(7F10.3)
      READ(5,102) HE,ZO,AFO,W
  102 FORMAT(4F10.5)
      READ(5,99) NO
   99 FORMAT(I3)
      WRITE(6,510) L1,L2,AP,SA,PO,C1,C2,HE,ZO,AFO,FDIA,FSP,W,N
  510 FORMAT(5X,4F10.5,/,5X,3F10.5,/,5X,3F10.5,/,5X,4F10.5,/,/)
C
      PNON=ROW*  FSP*FSP*FDIA*FDIA
      QNON=FSP*FDIA*FDIA*FDIA/AP
      TDIM=1./W
      IMT=20
      TT=10.
      HE=HE/12.
      ZO=ZO/12.
      DELO=2.*PHI*W
      TRS=TR
      NR=N-1.
      NP=NO-1
      NDUCT=(NO-1)/5
      NO5=NDUCT+1
      N10=2*NDUCT+1
      N15=3*NDUCT+1
      N20=4*NDUCT+1
      DELX=L1/NR
      D1=DSQRT(4.*AP/PHI)
      D2=DSQRT(4.*SA/PHI)
      DELT=DELX/2.5/VMAX
      SP=DSQRT(KP*G*R*TR)
      TETA=DELT/DELX
      CP=D2*PHI
      T=0.
      H=HE
      AO=H*CP
C
C
C     INITIAL CONDITIONS THROUGHOUT SYSTEM.
C     NONLINEAR EQUATIONS SOLVED BY A NEWTON RAPHSON ITERATION.
C
C     INITIAL GUESS.
      PF=60.
      PFO=50.
      PC=40.
      V=20.
    5 CONTINUE
      FF(1)=PF-PO-C1*V-C2*V*V
      FF(2)=PF-PFO-FR *L1*V*V*ROW/D1/2.
      FF(3)=PFO-PC-(V*AP/CD/AFO)**2*ROW/2.
      FF(4)=PC-(AP*V/AO/CD)**2*ROW/2.
      AA(1,1)=1.
      AA(1,2)=0.
      AA(1,3)=0.
      AA(1,4)=-C1-2.*C2*V
      AA(2,1)=1.
      AA(2,2)=-1.
      AA(2,3)=0.
      AA(2,4)=-FR *L1*V*ROW/D1
```

```
      AA(3,1)=0.
      AA(3,2)=1.
      AA(3,3)=-1.
      AA(3,4)=-(AP /CD/AFO)**2*V*ROW
      AA(4,1)=0.
      AA(4,2)=0.
      AA(4,3)=1.
      AA(4,4)=-(AP /AO/CD)**2*V*ROW
C     SUBROUTINE DMINV IS A MATRIX INVERSION SUBROUTINE FROM THE
C     U OF T COMPUTER CENTRE  SSP  SUBROUTINE LIBRARY.
      CALL DMINV(AA,4,DET,LL,M)
C     CORRECTION
      IR=0
      DO 10 J=1,4
      IR=IR+1
      XF(IR)=0.
      IC=0
      DO 10 I=1,4
      IC=IC+1
   10 XF(IR)=XF(IR)+AA(IR,IC)*FF(IC)
      PF=PF-XF(1)
      PFO=PFO-XF(2)
      PC=PC-XF(3)
      V=V-XF(4)
      SUM=0.
      DO 15 JJ=1,4
      SUM=SUM+DABS(XF(JJ))
   15 CONTINUE
      IF(SUM.LT..001  ) GO TO 20
      GO TO 5
   20 CONTINUE
      PCE=PC
      P(1)=PF
      VP(1)=V
      DO 25 II=2,NO
      P(II)=P(II-1)-ROW*FR*DELX*V*V/D1/2.
      VP(II)=V
   25 CONTINUE
      PCN=PCE/PNON
      TN=T/TDIM
      DO 26 IZ=1,NO
      PP(IZ)=P(IZ)
      VV(IZ)=VP(IZ)
      PN(IZ)=P(IZ)/PNON
      QN(IZ)=VP(IZ)/QNON
   26 CONTINUE
C
      WRITE(6,500) T,PP(1),PP(N05),PP(N10),PP(N15),PP(N20),PP(NO)
     *,PCE,VV(1),VV(N05),VV(N10),VV(N15),VV(N20),VV(NO)
      WRITE(6,500)TN,PN(1),PN(N05),PN(N10),PN(N15),PN(N20),PN(NO)
     *,PCN,QN(1),QN(N05),QN(N10),QN(N15),QN(N20),QN(NO)
  500 FORMAT(F12.7,2X,7F12.7,/,14X,6F12.7)
      DH=0.
      WRITE(6,505) H,DH,AO
  505 FORMAT(12X,3F20.10,/)
C
C
C     SOLUTION FOR DUCT FLOW BY THE METHOD OF CHARACTERISTICS.
C
      IN=0
   90 CONTINUE
C     FAN
      VS=(VP(1)-TETA*SP*(VP(1)-VP(2)))/(1.-TETA*(VP(1)-VP(2)))
      PS=P(1)+TETA*(VS-SP)*(P(1)-P(2))
   30 CONTINUE
      IF(VV(1).LE.0.) GO TO 747
      F1=PP(1)-PO-C1*VV(1)-C2*VV(1)*VV(1)
      A11=1.
      A12=-C1-2.*C2*VV(1)
      GO TO 707
  747 CONTINUE
      F1=PP(1)-PO
      A11=1.
      A12=0.
  707 CONTINUE
      F2=VV(1)-VS-R*TR*G*(PP(1)-PS)/(PS+2120.)/SP+FR*VS*DABS(VS)*DELT
     */D1/2.
      A21=-R*TR*G/(PS+2120.)/SP
      A22=1.
      DET1=A11*A22-A21*A12
      AF11=A22/DET1
      AF12=-A12/DET1
      AF21=-A21/DET1
      AF22=A11/DET1
      ER1=AF11*F1+AF12*F2
      ER2=AF21*F1+AF22*F2
      PP(1)=PP(1)-ER1
      VV(1)=VV(1)-ER2
      ERROR=DABS(ER1)+DABS(ER2)
      IF(ERROR.LT..001  ) GO TO 35
      GO TO 30
   35 CONTINUE
C     DUCT BETWEEN FAN AND FIXED ORIFICE.
      I=2
      D=D1
   40 CONTINUE
      VR=(VP(I)-(VP(I)-VP(I-1))*SP*TETA)/(1.+TETA*(VP(I)-VP(I-1)))
      VS=(VP(I)-TETA*SP*(VP(I)-VP(I+1)))/(1.-TETA*(VP(I)-VP(I*1)))
      PR=P(I)-TETA*(VR+SP)*(P(I)-P(I-1))
      PS=P(I)+TETA*(VS-SP)*(P(I)-P(I+1))
      VV(I)=.5*(VR+VS+R*TR*G*(PR-PS)/(P(I)+2120.)/SP-FR*DELT/2./D*
     *(VR*DABS(VR)+VS*DABS(VS)))
      PP(I)=.5*(PR+PS+(P(I)+2120.)*SP*(VR-VS)/R/TR/G-(P(I)+2120.)*SP*FR
     **DELT*(VR*DABS(VR)-VS*DABS(VS))/(R*TR*G*2.*D))
      IF(I.EQ.NP) GO TO 45
      I=I+1
      GO TO 40
   45 CONTINUE
C     FIXED ORIFICE
      PP(NO)=P(NO)
      VV(NO)=VP(NO)
      CFO=(CD*AFO/AP )**2*2./ROW
      VR=(VP(NO)-(VP(NO)-VP(NP))*SP*TETA)/(1.+TETA*(VP(NO)-VP(NP)))
      PR=P(NO)-TETA*(VR+SP)*(P(NO)-P(NP))
   60 CONTINUE
      F1   =CFO*(PP(NO)-PCE   )-VV(NO)*VV(NO)
      F2   =VV(NO)-VR+R*TR*G*(PP(NO)-PR)/(PR+2120.)/SP+FR*VR*DABS(VR)
     **DELT/2./D1
      A11=CFO
      A12=-2.*VV(NO)
```

```
      A21=R*TR*G/(PR+2120.)/SP
      A22=1.
      IF(VV(NO).GE.0.) GO TO 69
      F1=CFO*PP(NO)+VV(NO)*VV(NO)-CFO*PCE
      A12=2.*VV(NO)
   69 CONTINUE
      DET2=A11*A22-A21*A12
      AD11=A22/DET2
      AD12=-A12/DET2
      AD21=-A21/DET2
      AD22=A11/DET2
      ER1=AD11*F1+AD12*F2
      ER2=AD21*F1+AD22*F2
      PP(NO)=PP(NO)-ER1
      VV(NO)=VV(NO)-ER2
      SUM=DABS(ER1)+DABS(ER2)
      IF(SUM.LT..001  ) GO TO 80
      GO TO 60
   80 CONTINUE
      DO 85 J=1,NO
      P(J)=PP(J)
      VP(J)=VV(J)
      PN(J)=P(J)/PNON
      QN(J)=VP(J)/QNON
   85 CONTINUE
C
C
C     PLENUM PRESSURE BY RUNGE KUTTA INTEGRATION OF CONTINUITY EQN..
C
      PT=PP(NO)
      TCT=T
      PCT=PC
      Z=ZO*DSIN(TCT*DELO)
      H=HE+Z
      DZ=ZO*DELO*DCOS(TCT*DELO)
      DH=DZ
C     NOTE..TO REMOVE CHANGE OF PLENUM VOLUME WITH VARIATION OF
C     HOVER GAP, SET DH=0.. ALSO, SET VC=SA*(L2+HE).
      AO=H*CP
      QC=AFO*CD*G*DSQRT(2.*ROW*DABS(PT-PCT))
      IF((PT-PCT).LE.0.) QC=-QC
      QA=AO*CD*G*DSQRT(2.*ROW*DABS(PCT))
      IF(PCT.LE.0.) QA=-QA
      IF(AO.LE.0.) QA=0.
      VC=SA*(L2+H)
      PA=DELT*((QC-QA)*R*TRS*KP/VC-(PCT+2120.)*SA*KP/VC*DH)
      TCT=T+DELT/2.
      PCT=PC+.5*PA
      Z=ZO*DSIN(TCT*DELO)
      H=HE+Z
      DZ=ZO*DELO*DCOS(TCT*DELO)
      DH=DZ
      AO=H*CP
      QC=AFO*CD*G*DSQRT(2.*ROW*DABS(PT-PCT))
      IF((PT-PCT).LE.0.) QC=-QC
      QA=AO*CD*G*DSQRT(2.*ROW*DABS(PCT))
      IF(PCT.LE.0.) QA=-QA
      IF(AO.LE.0.) QA=0.
      VC=SA*(L2+H)
      PB=DELT*((QC-QA)*R*TRS*KP/VC-(PCT+2120.)*SA*KP/VC*DH)
      PCT=PC+.5*PB
      QC=AFO*CD*G*DSQRT(2.*ROW*DABS(PT-PCT))
      IF((PT-PCT).LE.0.) QC=-QC
      QA=AO*CD*G*DSQRT(2.*ROW*DABS(PCT))
      IF(PCT.LE.0.) QA=-QA
      IF(AO.LE.0.) QA=0.
      PD=DELT*((QC-QA)*R*TRS*KP/VC-(PCT+2120.)*SA*KP/VC*DH)
      TCT=T+DELT
      PCT=PC+PD
      Z=ZO*DSIN(TCT*DELO)
      H=HE+Z
      DZ=ZO*DELO*DCOS(TCT*DELO)
      DH=DZ
      AO=H*CP
      QC=AFO*CD*G*DSQRT(2.*ROW*DABS(PT-PCT))
      IF((PT-PCT).LE.0.) QC=-QC
      QA=AO*CD*G*DSQRT(2.*ROW*DABS(PCT))
      IF(PCT.LE.0.) QA=-QA
      IF(AO.LE.0.) QA=0.
      VC=SA*(L2+H)
      PE=DELT*((QC-QA)*R*TRS*KP/VC-(PCT+2120.)*SA*KP/VC*DH)
      PC=PC+1./6.*(PA+2.*(PB+PD)+PE)
      PCE=PC
      T=T+DELT
      IN=IN+1
      IF(IN.EQ.IMT) GO TO 400
      GO TO 401
  400 CONTINUE
      IN=0
      TN=T/TDIM
      PCN=PCE/PNON
      WRITE(6,500) T,PP(1),PP(N05),PP(N10),PP(N15),PP(N20),PP(NO)
     *,PCE,VV(1),VV(N05),VV(N10),VV(N15),VV(N20),VV(NO)
      WRITE(6,500)TN,PN(1),PN(N05),PN(N10),PN(N15),PN(N20),PN(NO)
     *,PCN,QN(1),QN(N05),QN(N10),QN(N15),QN(N20),QN(NO)
      WRITE(6,505) H,DH,AO
  401 CONTINUE
      TNON=T*W
      IF(TNON.LE.TT)  GO TO 90
      STOP
      END

STATISTICS -   330 CARDS READ,-   344 LINES PRINTED
```

UTIAS TECHNICAL NOTE NO. 211

Institute for Aerospace Studies, University of Toronto
4925 Dufferin Street, Downsview, Ontario, Canada, M3H 5T6

DUCT EFFECTS ON THE DYNAMIC FAN CHARACTERISTICS OF AIR CUSHION SYSTEMS

Hinchey, M. J. and Sullivan, P. A. 30 pages

1. Loops 2. Long ducts 3. Method of Characteristics

I. Hinchey, M. J., Sullivan, P. A. II. UTIAS Technical Note No. 211

During dynamic operation of an air cushion system, the fan operating point as seen at the cushion does not move along a static characteristic. Instead, it moves on a loop. Such loops have been observed experimentally by Durkin and Langhi (Ref. 1). This note shows that loop type behaviour can be predicted theoretically. The theory models the fan-duct-plenum system as a one dimensional acoustic vibration system. It uses the well known Method of Characteristics and a finite difference technique known as the method of specified time intervals to solve for the pressure and flow variations which occur along the duct during unsteady operation. Several practical situations where the loop behaviour may be of importance are discussed.

Available copies of this report are limited. Return this card to UTIAS, if you require a copy.

UTIAS TECHNICAL NOTE NO. 211

Institute for Aerospace Studies, University of Toronto
4925 Dufferin Street, Downsview, Ontario, Canada, M3H 5T6

DUCT EFFECTS ON THE DYNAMIC FAN CHARACTERISTICS OF AIR CUSHION SYSTEMS

Hinchey, M. J. and Sullivan, P. A. 30 pages

1. Loops 2. Long ducts 3. Method of Characteristics

I. Hinchey, M. J., Sullivan, P. A. II. UTIAS Technical Note No. 211

During dynamic operation of an air cushion system, the fan operating point as seen at the cushion does not move along a static characteristic. Instead, it moves on a loop. Such loops have been observed experimentally by Durkin and Langhi (Ref. 1). This note shows that loop type behaviour can be predicted theoretically. The theory models the fan-duct-plenum system as a one dimensional acoustic vibration system. It uses the well known Method of Characteristics and a finite difference technique known as the method of specified time intervals to solve for the pressure and flow variations which occur along the duct during unsteady operation. Several practical situations where the loop behaviour may be of importance are discussed.

Available copies of this report are limited. Return this card to UTIAS, if you require a copy.

UTIAS TECHNICAL NOTE NO. 211

Institute for Aerospace Studies, University of Toronto
4925 Dufferin Street, Downsview, Ontario, Canada, M3H 5T6

DUCT EFFECTS ON THE DYNAMIC FAN CHARACTERISTICS OF AIR CUSHION SYSTEMS

Hinchey, M. J. and Sullivan, P. A. 30 pages

1. Loops 2. Long ducts 3. Method of Characteristics

I. Hinchey, M. J., Sullivan, P. A. II. UTIAS Technical Note No. 211

During dynamic operation of an air cushion system, the fan operating point as seen at the cushion does not move along a static characteristic. Instead, it moves on a loop. Such loops have been observed experimentally by Durkin and Langhi (Ref. 1). This note shows that loop type behaviour can be predicted theoretically. The theory models the fan-duct-plenum system as a one dimensional acoustic vibration system. It uses the well known Method of Characteristics and a finite difference technique known as the method of specified time intervals to solve for the pressure and flow variations which occur along the duct during unsteady operation. Several practical situations where the loop behaviour may be of importance are discussed.

Available copies of this report are limited. Return this card to UTIAS, if you require a copy.

UTIAS TECHNICAL NOTE NO. 211

Institute for Aerospace Studies, University of Toronto
4925 Dufferin Street, Downsview, Ontario, Canada, M3H 5T6

DUCT EFFECTS ON THE DYNAMIC FAN CHARACTERISTICS OF AIR CUSHION SYSTEMS

Hinchey, M. J. and Sullivan, P. A. 30 pages

1. Loops 2. Long ducts 3. Method of Characteristics

I. Hinchey, M. J., Sullivan, P. A. II. UTIAS Technical Note No. 211

During dynamic operation of an air cushion system, the fan operating point as seen at the cushion does not move along a static characteristic. Instead, it moves on a loop. Such loops have been observed experimentally by Durkin and Langhi (Ref. 1). This note shows that loop type behaviour can be predicted theoretically. The theory models the fan-duct-plenum system as a one dimensional acoustic vibration system. It uses the well known Method of Characteristics and a finite difference technique known as the method of specified time intervals to solve for the pressure and flow variations which occur along the duct during unsteady operation. Several practical situations where the loop behaviour may be of importance are discussed.

Available copies of this report are limited. Return this card to UTIAS, if you require a copy.